CONTRIBUTIONS FROM THE MUSEUM OF PALEONTOLOGY

THE UNIVERSITY OF MICHIGAN

Vol. 25, No. 9, p. 169-219 (5 text-figs.; 17 plates). December 31, 1981

THE SKELETAL MORPHOLOGY OF THE ISOCRINID CRINOIDS *ANNACRINUS WYVILLETHOMSONI* AND *DIPLOCRINUS MACLEARANUS*

BY

D. BRADFORD MACURDA, JR.
AND
MICHEL ROUX

MUSEUM OF PALEONTOLOGY
THE UNIVERSITY OF MICHIGAN
ANN ARBOR

CONTRIBUTIONS FROM THE MUSEUM OF PALEONTOLOGY

Philip D. Gingerich, Director

Robert V. Kesling, Editor

Diane Wurzinger, Editor for this number

The series of contributions from the Museum of Paleontology is a medium for the publication of papers based chiefly upon the collection in the Museum. When the number of pages issued is sufficient to make a volume, a title page and a table of contents will be sent to libraries on the mailing list, and to individuals upon request. A list of the separate papers may also be obtained. Correspondence should be directed to the Museum of Paleontology, The University of Michigan, Ann Arbor, Michigan, 48109.

VOLS. II–XXV. Parts of volumes may be obtained if available. Price lists available upon inquiry.

THE SKELETAL MORPHOLOGY OF THE ISOCRINID CRINOIDS *ANNACRINUS WYVILLETHOMSONI* AND *DIPLOCRINUS MACLEARANUS*

By

D. Bradford Macurda, Jr.* and Michel Roux

Abstract.– The Recent isocrinid crinoids *Annacrinus wyvillethomsoni* (Wyville Thomson, 1872) from the eastern Atlantic and *Diplocrinus maclearanus* (Wyville Thomson, 1877) from the western Atlantic are similar in the calyx, length of the arms and morphology of the stem joints but differ strongly in the external morphology of their column. Study of the skeleton by scanning electron microscopy reveals some differences in cirral articulations, internal characteristics of the radials and basals, and non-muscular articulations of the arms, including lateral ligament fossae for bracing of the arms. Muscular articulations of the arms and pinnules are similar, as both species are rheophilic crinoids. Their stem joints are compared with the joints of the stalk of *Diplocrinus alternicirrus* (Carpenter, 1884). The ontogeny of the columnals suggests strong phylogenic relations between these three species. The differences in external morphology are interpreted as being of adaptative significance. *Annacrinus* is adapted for muddy substrates, *Diplocrinus* for rocky substrates or elevated living positions on sponges or alcyonarians. *Annacrinus* is herein ranked as a subgenus of *Diplocrinus*.

INTRODUCTION

The isocrinid crinoids first appeared in the Triassic and are locally numerous in Mesozoic limestones and shales. The Tertiary fossil record contains few representatives of these animals (characterized by a stalk with true cirri, a dicyclic cup with wide radial facets, and usually having uniserial arms); however, isocrinids are locally abundant now in the tropical western Atlantic and western Pacific at depths of a few to several hundred meters. The basic skeletal morphology of the isocrinids has been conservative since the Jurassic and therefore conclusions derived from the study of modern species should be applicable to fossil isocrinids.

There are five species of isocrinids in the tropical western Atlantic: *Cenocrinus asterius* (Linne, 1775), *Diplocrinus maclearanus* (Wyville Thomson, 1877), *Endoxocrinus parrae* (Gervais, 1835), *Isocrinus* (?) *blakei* (Carpenter, 1882), and *Neocrinus decorus* (Wyville Thomson, 1864) which have varying geographic ranges extending southward from the Bahamas into the Caribbean and rarely as far as Brazil (Meyer, Messing, and Macurda, 1978). There is one isocrinid in the eastern Atlantic, *Annacrinus wyvillethomsoni* (Jeffreys, nomen nudum; Wyville Thomson, 1872) which occurs from the Bay of Biscay to Morocco, the Canary Islands, and the Azores at depths of 1330 to 2002 meters (Clark, 1923). This article is the first of a series of comparative morphological studies of the Atlantic isocrinids: *Annacrinus wyvillethomsoni* and *Diplocrinus maclearanus* are examined herein because of their overall similarity. Macurda assumed primary responsibility for the study and interpretation

* Present address: The Energists, 5085 Westheimer, Apt. No. 7, Galleria II, Houston, Texas 77056

of the crown of each species while Roux did the same for the pelma. Roux (1976, 1977) discussed the growth and variability of a population of 520 individuals of *A. wyvillethomsoni* from the Gulf of Gascogne and made a comparative study of the stem joints of the Isocrinidae and has proposed modifications in systematics (he regards *Annacrinus* as a subgenus of *Diplocrinus*). Several SEM-photographs of arm and pinnular joints, muscular and collagenous fibers of *Annacrinus* have been presented in recent papers (Roux, 1974; Macurda, Meyer, and Roux, 1978). Macurda and Meyer (1976) have illustrated and interpreted the life mode of *D. maclearanus*, and Meyer, Messing, and Macurda (1978) detailed the geographic occurrence of this species.

EXTERNAL MORPHOLOGY

The external morphology of *D. maclearanus* (Pl. 1, figs. 1, 6) was studied by measuring 15 characters on 60 individuals from six of the seven stations listed by Meyer, Messing, and Macurda (1978). The mean and standard deviation of these are listed in Table 1. Because of postmortem curling of arms, stalks, and cirri, some measurements (stem length, cirral length, arm length, height of crown) are accurate only to 5-10 mm on individual specimens. *D. maclearanus* has one of the shortest columns ($\bar{x}$ = 41.7 mm) of any isocrinid crinoid when compared to arm length ($\bar{x}$ = 66.9 mm; crown length $\bar{x}$ = 76.7 mm) and the highest ratio of nodal to internodal plates (1:4.8). The cirri are long ($\bar{x}$ = 30.4 mm); this combined with the numerous nodals produces a dense forest of cirri for grasping onto substrates. Macurda and Meyer (1976) noted it used the cirri to grasp alcyonarians, sponges, or rocky substrates. The number of cirrals in each cirrus is rather constant (26.5). The calyx (consisting of basals and radials) is small and the correlation (r = 0.36) between height ($\bar{x}$ = 2.0 mm) and width ($\bar{x}$ = 7.4 mm) is low. Arms ($\bar{x}$ = 24.5 mm) usually number either 4, 5, or 6 per ray and each half ray branches endotomously when three arms are present. A few very large individuals had up to four arms per half ray (endotomous). A few isolated occurrences of the bifurcation of an inner arm were also noted. The average number of arms per individual is 24.5 (n = 38; $s_{\bar{x}}$ = 3.8). The greatest number of arms in any complete individual was 31. The correlation between stem length and crown height was intermediate (r = 0.60) while that between pinnule length ($\bar{x}$ = 12.1 mm) and number of pinnulars was higher (r = 0.72).

Roux (1976) reviewed the biometry of *A. wyvillethomsoni* (Pl. 7, figs. 1, 8) and noted that it was one of the smaller isocrinids. Of the 520 specimens available to him, 256 had well-preserved crowns and 310 well-preserved columns. The mean length of the stem was 108.8 mm, of the crown 69.9 mm. The number of arms ranged from 10 to 21 with a mean of 16.6. Thus the column is longer, the crown smaller, and the number of arms less than in *D. maclearanus*. In addition, the number of internodals is much larger and they are undifferentiated in size compared to *D. maclearanus*. The cirri are shorter and much less numerous. During the growth of *Annacrinus*, additional arms appear because of regeneration and then, sometimes, the arm division number is aberrant (one IBr or IIIBr, three IIBr).

CALYX

The calyx of *D. maclearanus* consists of five basals and five radials. The basals have limited external exposure, being indented on the lower surface by columnals and overlapped on the upper surface by the radials which they alternate with. The outer lower surface of each basal has a lip which projects downward over a columnal, thereby providing a firmer lock between the column and calyx. The lower indented surface of the basal has four culmina on each side of the petaloid areola (Pl. 1, figs. 2, 3). The stereom of the areola is galleried with pores approximately 0.01 mm in diameter. A few larger diameter pores (0.03 mm) border the areola; these are regularly spaced and are apparently continuous with canals within the columnals. The stereom of the culmina is irregular.

TABLE 1 – Summary of morphological variables of *Diplocrinus maclearanus* (Wyville Thomson, 1877) n=60 except number of arms where n=38. Measurements in mm.

Variable	Mean ($\bar{x}$)	Standard Deviation (s_x)
Column length	41.7	14.5
Diameter of internodal	3.5	0.6
Number of mature nodals	6.0	2.4
Number of immature nodals	2.0	0.7
Number of internodals	4.8	0.5
Cirral length	30.4	5.3
Number of cirral plates	26.5	2.2
Diameter of cirral plate	1.1	0.2
Height of calyx	2.0	0.3
Width of calyx	1.4	0.9
Length of arms	66.9	11.3
Length of crown	76.7	11.7
Diameter of brachials	1.9	0.3
Number of arms	24.5	3.8
Number of pinnulars	15.4	1.9
Length of pinnule	12.1	2.0

Each innermost lower face of the five basals forms a part of the border to the continuation of the axial canal (Pl. 1, fig. 9). An open stereom with many pointed dagger-like extensions fills the axial canal in the central and upper part of the inner face of the basal. Peripheral to this, the axial canal subdivides into two nerve canals which emerge on the inner part of the upper surface of each basal. The lumen of each canal has a diameter of 0.14 mm. The upper and lateral surface of each basal has a dense irregular stereom.

A calyx of *A. wyvillethomsoni* also consists of five basals and radials. The outer lower edge of the basal lacks the lip seen in *D. maclearanus* but is instead slightly concave. The basal is more visible and continuous in lateral view. The lower surface is indented with an areola which has galleried stereom (Pl. 7, figs. 4, 5). The areola is bordered by two culmina on each side. The larger (accessory?) nerve canals are only present on the inner third of the basal. It is in the concave area on the lower surface of all five basals that new columnals are initially formed and undergo expansion to a mature age (Pl. 7, figs. 2, 3). The middle and upper part of the axial canal is again filled with stereom (Pl. 7, figs. 6, 7); this is denser in *A. wyvillethomsoni*. The peripheral subdivision of the axial canal into two nerve canals which emerge on the inner upper edge of each basal occurs at a lower point on the inner face of the basal.

The upper edge of the radial of *D. maclearanus* bears a large muscular articulation. The area of the dorsal ligament fossa is the largest and has galleried stereom; the ventral ligament fossae are also galleried but smaller in area. The muscle fossae are well differentiated. The stereom in the lower, inner part of each fossa is more elevated and has a more irregular surface than that in the rest of the fossa. The lateral edges of each radial have an opening for the lateral nerve ring (diameter 0.17 mm)

and some culmina along the upper edge of the surface which help to strengthen and rigidify the contact between the radials (Pl. 1, figs. 4, 5). The lower surface of the radial is divided by a sharp median ridge and each half is slightly concave where it fits against the upper convex surface of the basal. Nerve canals from adjacent basals penetrate into the inner lower surface of the radial and continue upward to merge as a single ellipsoidal lumen on the upper surface on the muscular articulation (diameter 0.42 by 0.21 mm). The inner edge of the radial bears a groove between two ridges which splays into several smaller grooves as the basal is approached (Pl. 1, figs. 7, 8); these same grooves are also present on the uppermost part of the inner surface of the basal. It is unknown what tissue or organ is located within these spaces (chambered organ?).

The radials of *A. wyvillethomsoni* are similar in their configuration to those of *D. maclearanus*. The dorsal ligament fossa is not as large relative to the rest of the radial facet and the muscle fossae are larger; stereom in the lower inner part of each muscle fossa is again differentiated from that in the rest. The latter shows concentric banding, probably produced by upward growth (Pl. 8, figs. 1, 2). The diameter of the lateral nerve canal is 0.25 mm, of the nerve canal entering the base of the radial 0.23 mm, and the elliptical lumen on the muscular articulation 0.43 by 0.23 mm. Culmina are again present along the upper part of the surface of contact between adjacent radials. The inner face of each radial is concave, with irregular knobs of stereom as one approaches the basals (Pl. 7, figs. 9, 10). The five radials thus frame a cylindrical space with irregular projections extending into it. This configuration is different than that of *D. maclearanus*.

ARMS

The base of each arm in *D. maclearanus* is comprised of two primibrachials, IBr_1 and IBr_2. IBr_1 articulates with the radial by means of a muscular articulation. The articular ridge is not sharply defined. Each lateral face of an IBr_1 has a depressed ligamentary fossa which provides ligamentary bonding to the adjacent IBr_1 and thus between the full circle of the five IBr_1. These five plates form a circle atop the radials and are at the base of the arm series. They are thus rigidified laterally with respect to one another to provide greater structural integrity to the base of the arm series at the point where the arms articulate with the calyx. The distal surface of IBr_1 is a rather featureless surface (Pl. 1, figs. 10, 11); there is no distinct articular ridge. There is a broad elevated area which runs horizontally across the surface, and the surface of the plate slopes gradually inward both dorsally and ventrally, producing a slightly convex distal surface on IBr_1. The stereom of the broad elevated area (Pl. 2, fig. 1) is less porous than that of the surrounding areas. The stereom of the latter is irregular, no regular galleries are present (Pl. 2, fig. 4).

The proximal surface of IBr_2 conforms to the surface of distal IBr_1, being slightly concave with the axis of concavity being horizontal. The function of this ligamentary articulation is to stiffen the base of the arm. Because it is a non-movable articulation, has a smooth surface, and short ligamentary fibers, it is best described as a synostosial articulation. The surfaces of this articulation on both IBr_1 and IBr_2 show concentric growth lines around the central nerve canal. The distal surface of IBr_2 is an axillary with two muscular articulations. The inner muscle fossae are reduced in surface area. The diameter of the elliptical lumen is 0.31 by 0.20 mm on these muscular articulations.

The base of each arm of *A. wyvillethomsoni* is also composed of an IBr_1 and IBr_2. The proximal surface of IBr_1 (Pl. 8, figs. 3, 4) has a well-developed muscular articulation. The fulcral ridge is sharply defined; the muscle fossae are much larger and more sharply defined than in *D. maclearanus*. The inner part of each muscle fossa is more elevated than the surrounding outer part of the fossa. Concentric growth lines ornament the latter. There are no lateral ligament fossae which would serve to rigidify the IBr_1 as there is in *D. maclearanus*. The distal surface of IBr_1 (Pl. 8, figs. 5, 6) is a rather smooth convex surface except for culmina bordering the articulation along its lower edge, making it a cryptosyzygy. The distal surface is convex in a vertical sense (Pl. 8, fig. 7) (highest

medially, recurving laterally) while the distal surface of IBr_1 of *D. maclearanus* is convex in a horizontal sense (highest in a medial horizontal position, recurving orally and aborally).

The proximal surface of IBr_2 of *A. wyvillethomsoni* conforms to that of the distal IBr_1; it is vertically concave and culmina are present along the outer border of the lower half of the facet (Pl. 8, figs. 8, 9). The distal surface of IBr_2 (Pl. 9, figs. 2, 3) is an axillary with two muscular articulations similar to those of *D. maclearanus* but the dorsal ligament fossa is narrower and the muscle fossae relatively larger. The diameter of the elliptical lumen is 0.35 by 0.20 mm on these muscular articulations.

The division series of the secundibrachials of *D. maclearanus* are two: two $IIBr_1$ and $IIBr_2$ follow each axillary IBr_2. The proximal surface of $IIBr_1$ is a muscular articulation but is asymmetric because of the necessity of articulating with the asymmetric muscular articulation of the axillary. A depressed ligament fossa is present on the inner edge of each $IIBr_1$, thus providing a ligamentary bonding between adjacent pairs of $IIBr_1$, and thereby bracing the base of the arm network. The distal surface of $IIBr_1$ (Pl. 2, figs. 2, 3) corresponds to the distal surface of IBr_1. The convexity of $IIBr_1$ is again horizontal; the center of curvature lies near the median of the plate instead of a more oral position. There is a development of faint culmina at the edge of the lower half of the facet. The stereom around the nerve canal is galleried but beyond this the stereom becomes dense and irregular (Pl. 2, figs. 7, 8). The concave proximal surface of $IIBr_2$ (Pl. 2, figs. 5, 6) conforms exactly to that of $IIBr_1$; the articulation is perhaps best described as a cryptosyzygy. The distal surface of $IIBr_2$ is an axillary (unless branching has not occurred as in some immature individuals). The muscular articulations on distal $IIBr_2$ (Pl. 2, figs. 9, 10) are narrower than those on IBr_2. The stereom of the central part of the dorsal ligament fossa is galleried as that of the ventral ligament fossae. The stereom of the muscle fossa is labyrinthic with small needle-like stereomic extensions perpendicular to the surface. It is more recessed than the surface of the ventral ligament fossa (Pl. 3, figs. 1, 2). As on other muscular articulations, the intermuscular furrow separates the muscle fossae and extends dorsally to the region of the ventral ligament fossae but does not extend as far as the lumen of the nerve canal; the diameter of the latter is 0.23 by 0.20 mm.

The division series of the secundibrachials of *A. wyvillethomsoni* are also two (unless an arm hasn't subdivided ontogenetically). The proximal surface of $IIBr_1$ (Pl. 9, figs. 5, 6) is an asymmetric muscular articulation which articulates with the axillary IBr_1. The fulcral ridge is well defined; the pores of the dorsal ligament fossa appear smaller than those of the ventral ligament fossa. The muscle fossae are slightly larger than those of the proximal $IIBr_1$ of *D. maclearanus*. There is a small ligament fossa on the inner side of the $IIBr_1$ (Pl. 9, fig. 1) which bonds it to the adjacent $IIBr_1$ arising from the same axillary. This fossa is much smaller than the corresponding lateral facet on the side of the $IIBr_1$ of *D. maclearanus*. The distal surface of the $IIBr_1$ (Pl. 9, figs. 8, 9) of *A. wyvillethomsoni* is a cryptosyzygy whose configuration corresponds to that of the distal surface of IBr_1. The upper (oral) part of the articulation is more extensively developed, and recurves distally. This distal surface fits tightly against the proximal surface of $IIBr_2$. The distally recurved upper surface of $IIBr_1$ fits into a corresponding reentrant on $IIBr_2$ (Pl. 9, fig. 10) and may serve to impart greater rigidity to the articulation. The muscular articulations of the distal surfaces of the axillary $IIBr_2$ (Pl. 9, figs. 11, 12) correspond to those of distal IBr_2. They are narrower than the latter and the articulation bordering the inner half of the ray is fifteen percent narrower than that on the outer half. The diameter of the nerve canal is 0.27 by 0.23 mm.

There may be subsequent division series in mature *D. maclearanus*. The distal $IIIBr_1$ surface is very slightly convex and the proximal $IIIBr_2$ very slightly concave. The surface lacks any obvious culmina and is thus a synostosial articulation.

The arms of *D. maclearanus* are composed of uniserial brachials. The first (Br_1) has an asymmetric proximal muscular articulation (Pl. 3, figs. 3, 4) where it articulates with $IIBr_2$. The lateral ligament fossa (Pl. 3, figs. 6, 7) is large, binding the brachial either to an adjacent brachial arising from the

same axillary or a $IIIBr_1$ or $IVBr_1$ arising from the same axillary. The stereom is galleried with pore diameters of 0.015 to 0.025 mm. The fulcral ridge of the muscular articulation is oblique and the area of the muscle fossae comprise about 50 percent of the articulation as opposed to about 25 percent on the proximal surface of IBr_1. The muscle fossa has labyrinthic stereom with short stereomic extensions on the surface (Pl. 3, fig. 8). The ventral and dorsal (Pl. 3, fig. 5) ligament fossae are galleried; pore diameters are 0.01 to 0.02 mm. The distal surface of Br_1 is a rather flat surface, being very slightly concave along a vertical axis and very slightly concave along a horizontal axis at the lower margin of the articulation. There are very faint irregular ridges at the edges of the articulation but they are too indistinct to qualify as culmina; therefore the suture is best termed a cryptosyzygy. The diameter of the nerve canal is 0.23 by 0.12 mm. All succeeding distal articulations within the arm are muscular articulations with oblique fulcral ridges (Pl. 3, figs. 9, 10) which alternate in their direction of slant. The fossae and fulcral ridge are well differentiated. Stereomic microstructure corresponds to that of proximal Br_1.

The brachials of *A. wyvillethomsoni* are also uniserial. The proximal surface of Br_1 (Pl. 9, fig. 4) is an asymmetric muscular articulation which attaches to an axillary. There is a small ligament fossa on the lower inner edge of the brachial which ties it to the adjacent brachial or IIBr of the ray series. The ears of the muscle fossae are much more elongated than on proximal IBr_1 and the relative area of the muscle fossae is increased. The differentiated stereom in the lower inner part of the muscle fossa is not as extensive as that on proximal IBr_1. The distal surface of Br_1 is very slightly convex and there are low culmina along the lower and lateral margins of the articulation; the latter are more irregular in their form. The slightly concave proximal surface of Br_2 (Pl. 9, fig. 7) fits tightly against distal Br_1, providing a stiffening joint at the base of the arm. The stereom of the smooth inner part of the articulation is galleried, that of the culmina and the area between them irregular. The diameter of the nerve canal is 0.40 by 0.16 mm. All succeeding articulations are muscular. The first pinnular articulation occurs atop Br_2.

The brachial articulations of *A. wyvillethomsoni* are well differentiated with an oblique fulcral ridge and large muscle fossae (Pl. 10, figs. 1-4). The fulcral ridge is slightly recurved at one end, perhaps implying an enhanced ability to twist the arm. The dorsal ligament fossa is galleried (pore diameters 0.008-0.015 mm) as are the ventral ligament fossae (pore diameters 0.012-0.025 mm). The muscle fossae are labyrinthic with small knobs projecting off the surface of the stereom (Pl. 10, figs. 8, 9). Pore diameters vary from 0.008 to 0.020 mm. The nerve canal is 0.23 by 0.20 mm. At the distal end of the arms, the configuration of the muscular articulations are modified (Pl. 11, figs. 1-4). The area occupied by the muscle fossae is reduced from over 40 percent to less than ten percent and the prominent ventral development is lacking. These distal brachials are nearly as long as the more proximal brachials but are thinner, producing a more elongate outline. The proximal end of the distal brachial is narrower than the distal end. The diameter of the nerve canal is 0.14 by 0.12 mm.

PINNULES

A pinnular-brachial articulation is located on the upper (ventral) surface of Br_2 and each succeeding brachial (Pl. 4, figs. 1, 2). They alternate along each side of the midline on succeeding brachials. In *D. maclearanus*, the pinnular articulation is muscular; there is a well-defined fulcral ridge, deep ligament pit in the dorsal ligament fossa, galleried pores in the dorsal and ventral ligament fossae, and a single deep muscle fossa. The last-named is the most distal part of the articulation. The diameter of the nerve canal is 0.08 by 0.06 mm. Pore diameters are 0.013-0.031 mm in the dorsal ligament fossa, 0.011-0.020 mm in the ventral ligament fossae. The proximal articulation of the proximal pinnular (P_1) is asymmetric, conforming to the surface on the brachial. The articulation between P_1 and P_2 is a more symmetric muscular articulation with a straight fulcral ridge and well-differentiated muscle fossae. Succeeding articulations are also muscular but the fossae are smaller

and the fulcral ridge has assumed a V-shaped configuration below the nerve canal (Pl. 4, figs. 3-10). The central part is protuberant on one surface, recessed on the opposing (distal) surface of a pinnular, thereby providing a firmer rotational surface. The stereom of the ligamental areas is galleried. Pore diameters are 0.010 to 0.027 mm. Individual pinnulars are elongate and trough shaped, with roofing cover plates (Pl. 17, figs. 8-11). Pinnules are long ($\bar{x}$ = 15.4 mm).

The pinnular-brachial articulation of *A. wyvillethomsoni* is also a muscular articulation (Pl. 10, figs. 5-7). There is a distinct, well-developed fulcral ridge (Pl. 11, figs. 5, 6). On distal brachials, the articulation is rather flat (Pl. 11, figs. 7, 8), the dorsal and ventral fossae are galleried, and the development of the muscle fossa is very small. In more proximal brachials, there is considerably more relief on the articulation due to its greater differentiation, the dorsal ligament pit is prominent, and the muscle fossa is relatively much larger and deeper. The diameter of the nerve canal is 0.06 mm on distal brachials, 0.10 mm on more proximal brachials. The proximal surface of the first pinnular, P_1 (Pl. 12, figs. 2, 3), is again asymmetric whereas the articulation between P_1 and P_2 is a nearly symmetrical muscular articulation with galleried stereom in the ligament fossae and labyrinthic stereom in the muscle fossae (Pl. 12, figs. 5, 6, 9). The shape of muscular articulations between subsequent pinnulars (Pl. 13, figs. 2, 3, 5, 6) is modified so that the fulcral ridge becomes more V-shaped and is less continuous, especially toward the edge of the facet. The size of the muscle fossae declines distally (Pl. 13, fig. 1); there is a small projecting spine at the dorsal edge of distal surfaces. The pinnulars are elongate and trough shaped, with roofing cover plates (Pl. 13, figs. 7, 8; Pl. 17, fig. 12). The first oral pinnule is similar (Pl. 12, figs. 1, 4, 7, 8, 10-13) but articulations of medial pinnulars therein are modified so that the articular ridge (which is broader and more diffuse) is more oblique to the V-shaped trough on the upper surface of the pinnular.

STEM

The external morphology of the columns of the two species studied in detail differs considerably. That of *Diplocrinus maclearanus* is characterized by a number of internodals per nodaxis which generally does not exceed five. Furthermore, the columnals are invariably stellate or pentagonal, their varying diameter reflecting their order of development: the first is situated between two nodals, followed by two which are juxtaposed with respect to the nodals and, finally, two other situated on either side of the first order internodal (text-fig. 1). On the other hand, *Annacrinus wyvillethomsoni* generally possesses several dozen internodals per nodaxis which rapidly become pentagonal or circular, having a uniform diameter and thickness. Only the proximal part of the stem exhibits a stellate cross section and a varying columnar diameter.

The symplexies of the two species (Pl. 15, figs. 2-7, 9, 10; Pl. 17, figs. 1-7) are characterized by an open crenularium (the lanceolate areola clearly extend to the external edge of the articulation) and a reduced number of culmina (generally 5-8). The synostosis of each (Pl. 15, fig. 8; Pl. 16, figs. 1-4, 7-12) have a reduced crenularium whose stereom consists of a β-type syzygial network with an axial canal which is often completely blocked (Roux, 1977). The morphology and microstructure of the articulations are summarized (Table 2) and compared with those of *Diplocrinus alternicirrus* (Carpenter) (Pl. 16, figs. 5, 6). It is noted that among the fourteen characteristics expressed by the three species, nine are peculiar to *A. wyvillethomsoni*, seven are common to *D. maclearanus* and *D. alternicirrus*, while only two are common to *D. maclearanus* and *A. wyvillethomsoni* and two to *D. alternicirrus* and *A. wyvillethomsoni*. These observations suggest that the species *wyvillethomsoni* belongs to the subgenus *Annacrinus*. The third known species of the genus *Diplocrinus* – *D. sibogae* Doderlein – seems to possess a column very comparable to that of *D. maclearanus* according to Doderlein's description (1907).

The biometry of the stereom of the lanceolate areola is very significant (Table 3). The radial curves (text-fig. 2) of *D. maclearanus* exhibit a localization of the biggest meshes within the inner

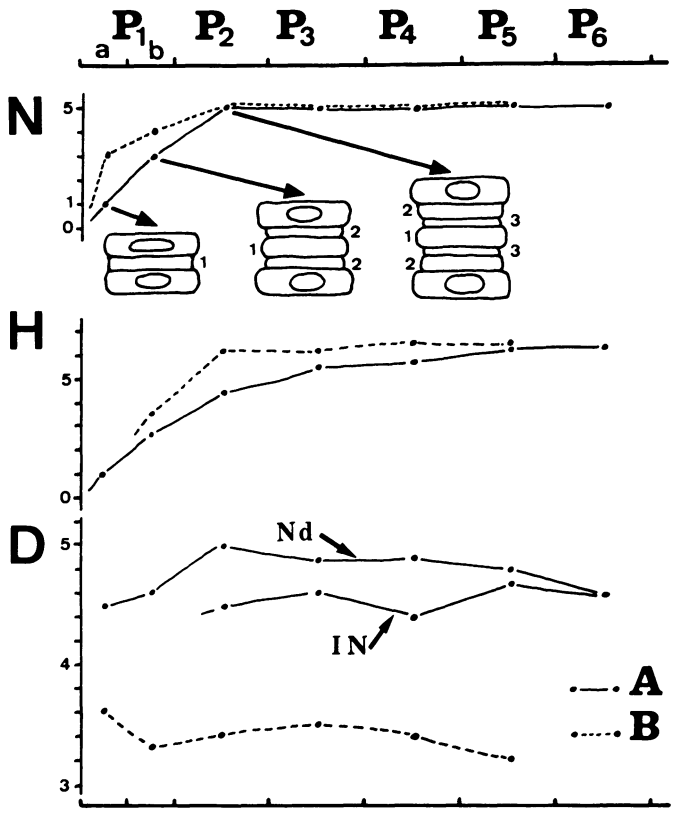

TEXT-FIG. 1 – Growth of the stem of *Diplocrinus maclearanus*. N: number of internodals; H: height of the nodotaxis; D: diameter of the columnal (Nd: nodal, IN: internodal); P: nodotaxis from the proximal part of the stem to the distal one (Pl: proximal part of the stem; P2: first nodotaxis with 5 internodals); A: old specimen 0 4226; B: specimen G 386.

part of the areola. This property is less marked in *D. alternicirrus* and barely visible in *A. wyville-thomsoni*. The decrease of the growth limit (level) of the diameter of the mesh with increasing age and the distal position of the columnals (Roux, 1971) is clearly expressed only in this latter species.

Comparative analysis of the internal diameter of the areola meshes (proportional to the diameter of the collagenous elastic fibers which penetrate into the ossicle) indicates that during the ontogeny different modifications appear (text-fig. 3). In *A. wyvillethomsoni*, the lowering of the maximum size of the diameter of the areola mesh strongly influences the nature of the frequency histograms as well as the evolution of the average size which tends towards lower values. However, the internal diameter of the mesh is invariably distributed in a homogeneous manner on the surface of the areola. In *D. maclearanus*, beginning from the proximal columnals, the frequency histograms are clearly asymmetric and one can already observe a considerable concentration of high values within the inner half of the areola (text-figs. 3-4). On the oldest columnals the average increases considerably, the asymmetry of the frequency histogram tending to be less marked but the segregation of the widest internal mesh diameter is very marked within the inner third of the areola.

The most probable interpretation is that the morphological differentiation in *D. maclearanus* allows a greater mobility of articulation. The large collagenous fibers concentrated near the axial canal assure the cohesion of the column and probably facilitated articulation between the columnals.

TABLE 2 – Characters of the joints in the stem of the genus *Diplocrinus*.

Characters			*D. maclearanus*	*D. alternicirrus*	*D. wyvillethomsoni*
synostosis	crenularium	stereom	syzygial-type β	syzygial-type β	culmen: syzygial-type β groove: synostosial-type β
		morphological feature	irregular, less marked	irregular, less marked	regular, well marked
	lumen	filling in	thick spicules	thin spicules	network
		shape	round	pentagonal	pentagonal
	interpetaloid zone	symmorphy	important but irregular	important and regular	rarely developed
		microstructural differentiation	not clear	slightly marked	well marked
symplexy	crenularium	inner crenularium	slightly differentiated on old columnals only	not clearly differentiated	slightly differentiated
		organization	often irregular	regular	regular and tend towards radial axes on distal or old columnals
		number of culmina	6–8	7–9	5–7
	interpetaloid zone	morphological feature	sometimes interlocked with the areola edge	covered by the crenularium	covered by the crenularium
		on proximal columnals	groove with classic β stereom	not observed	without groove, synostosial β stereom
		perilumen	calcitic thickness (function such as a pivot)	calcitic thickness (function such as a pivot)	never calcitic thickness
transversal cross section of a columnal under a symplexy		edge of the axial lumen	thick calcitic meshes	thick calcitic meshes	never differentiated
		under the inner crenularium	calcitic thickness	thick calcitic stereom with little meshes	calcitic thickness especially in old columnals
		perilumen	not thick calcitic stereom	thick calcitic stereom with little meshes	not thick calcitic stereom
cirrus joints		morphological feature of proximal joints	nearly bilateral symmetry	nearly bilateral symmetry	important bilateral dissymmetry
		shape of the facet of the proximal part	a few elliptical	a few elliptical	strongly elliptical

TABLE 3 – Size of the stereom meshes of the columnals in *Diplocrinus*.

network	α stereom most frequent size	average	β stereom most frequent size	average
D. wyville thomsoni	15–30 μ	23,5 μ	20–60 μ	32,7 μ
D. macleranus	20–40 μ	28 μ	25–65 μ	42,8 μ
D. alternicirrus	15–35 μ	23 μ	25–55 μ	34,3 μ

A similar observation has been made concerning the column of the Jurassic *Pentacrinus* (*Extracrinus*) and *Seirocrinus* (Roux, 1975). It is of considerable interest to note the morphological convergence between *D. macleranus* and *Pentacrinus dargnesi* Terguem and Jourdy, crinoids belonging to different taxa but probably adapted to comparable biotopes. The column of *A. wyvillethomsoni* has evolved differently by adapting to muddy substrates and possibly to rapid sedimentation (Roux, 1976, 1977). The column exhibits some aspects of convergence with certain Jurassic species of *Balanocrinus* which occur in muddy facies.

From a microstructural point of view, the perilumen and the internal crenularium of the columnals in *D. alternicirrus* (Pl. 14, fig. 9) appear to be only weakly evolved and their properties (stereom characterized by a thick calcitic network enclosing narrow internal voids) are equally present on the young columnals of *A. wyvillethomsoni*. Other columnals of this latter species, and all columnals in *D. macleranus* (Pl. 14, fig. 8) possess a perilumen which is distinctly separated microstructurally from the internal crenularium (text-fig. 5).

CIRRI

The cirri of *Diplocrinus macleranus* are closely spaced. The cirral articulation on a nodal is a depressed oval with a fulcral ridge on either side of the nerve canal which gives way to two large knobs laterally (Pl. 5, figs. 1, 2; Pl. 15, fig. 1). The stereom is galleried both above and below the ridge and knob, and pore diameters range from 0.01-0.02 mm. The fossae are slightly concave. The proximal surface of the first cirral (Pl. 5, figs. 3, 4) is slightly convex and the fulcral ridge is the most elevated

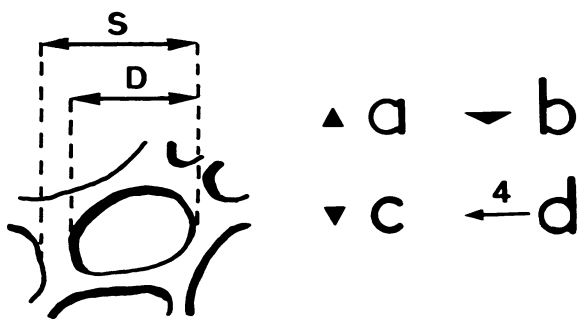

TEXT-FIG. 2 – Biometric radial curves of the columnals. *2a*: s: size of the stereom mesh; D: inner diameter of the mesh; a: growth center in development; b: growth level (the end of the development of a growth center); c: lowering of the growth level; d: growth level.

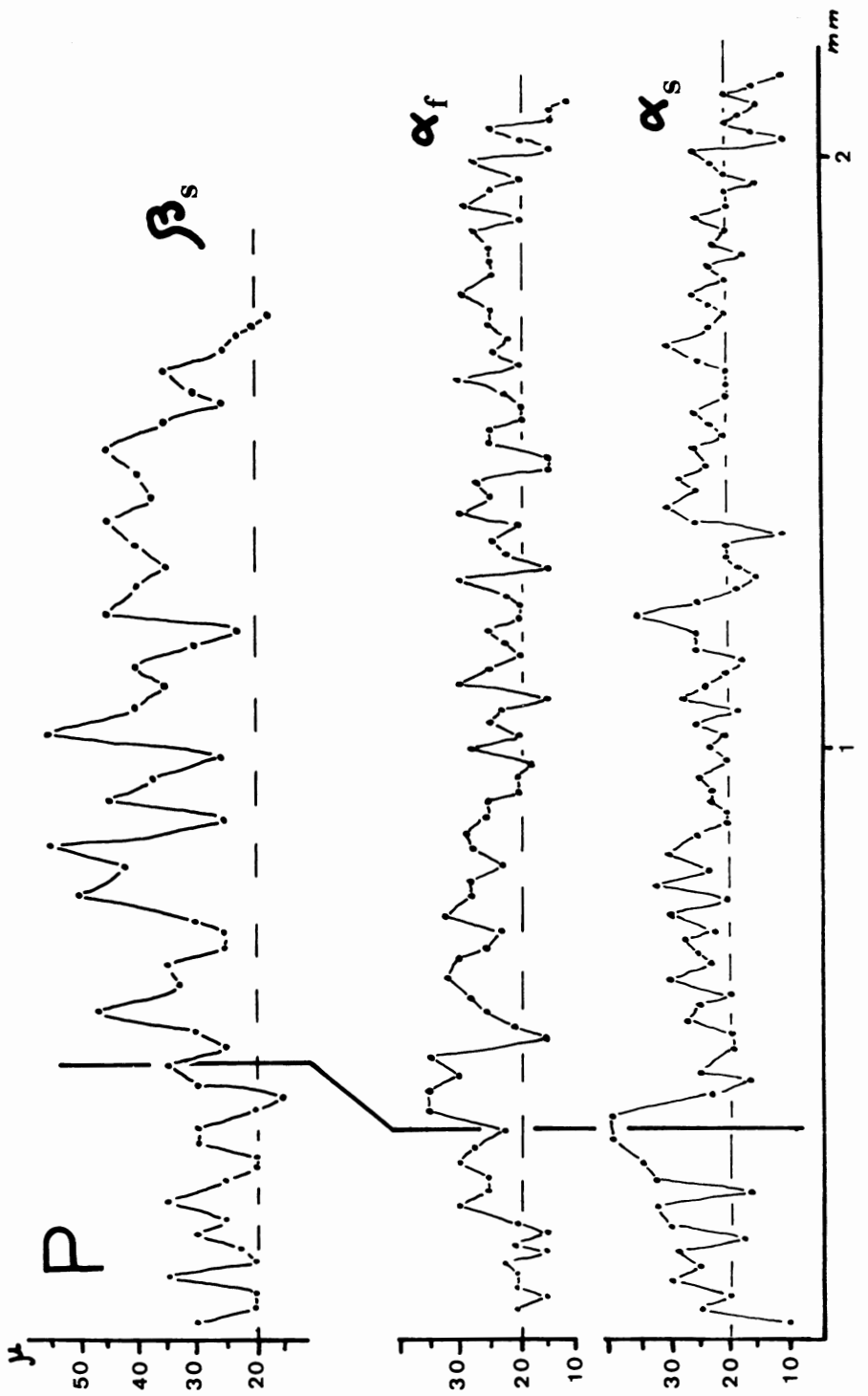

TEXT-FIG. 2 – *2b : Diplocrinus alternicirrus*. See α f and α s curves without clear growth level.

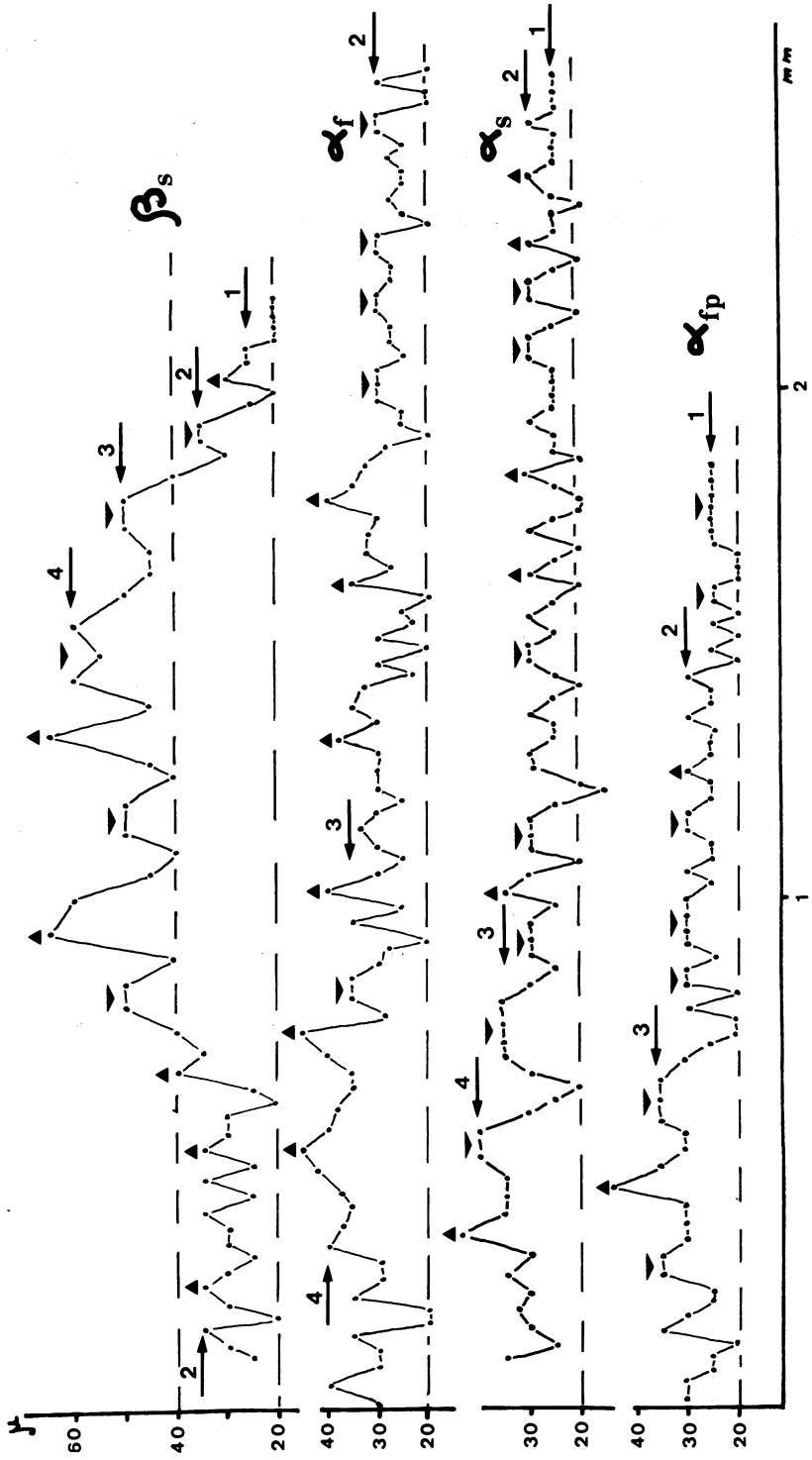

TEXT-FIG. 2 – *2c : Diplocrinus macleranus* (sp. 0 4226). Note the well marked growth levels for α and β radial curves.

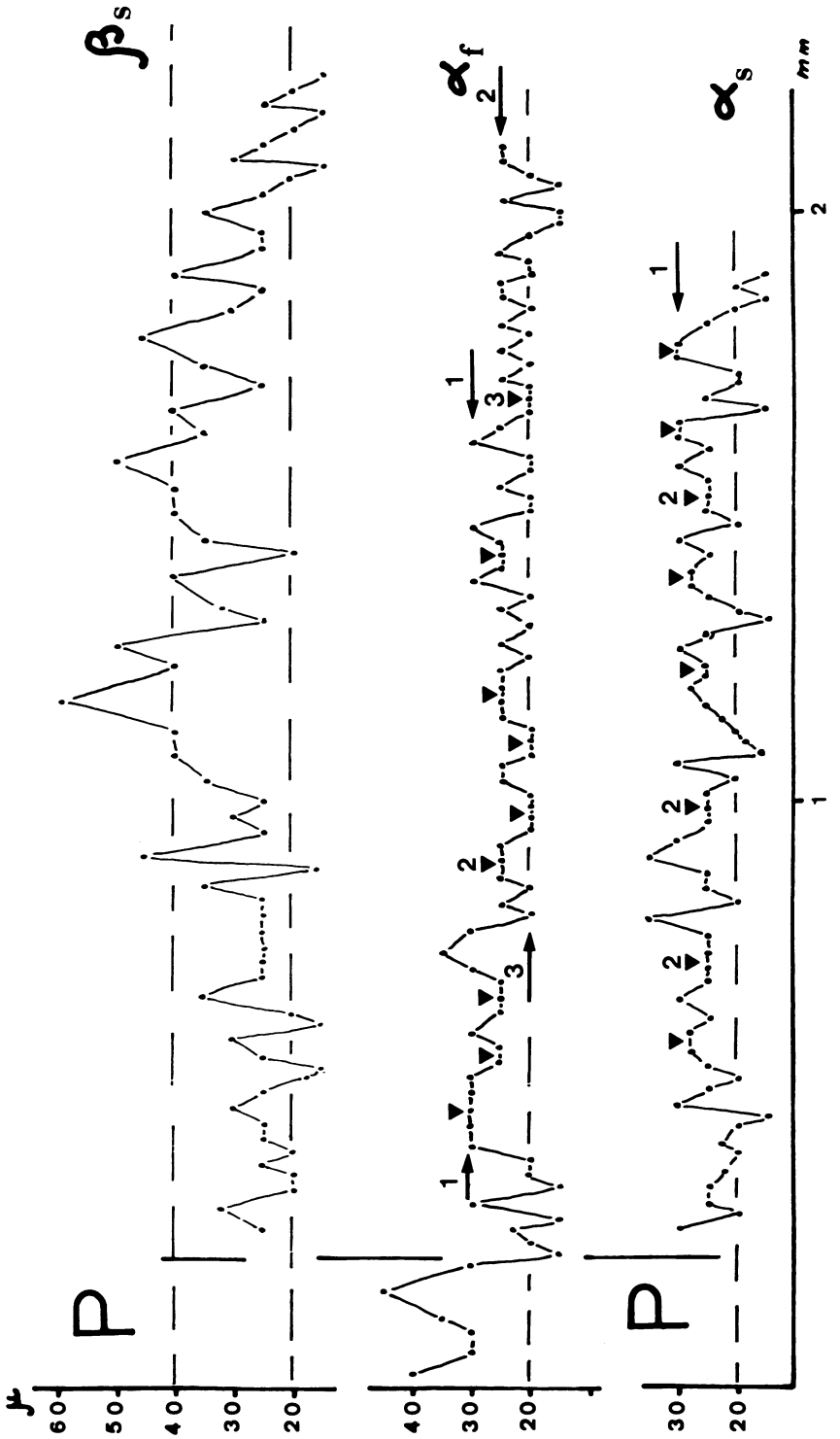

TEXT-FIG. 2 – *2d : D. (Annacrinus) wyville thomsoni* (sp. 331). Note growth levels of α stereom and the lowering of it during ontogeny. β s: β stereom in transverse cross section under the facet. α s: α stereom in transverse cross section under the facet. α f: α stereom of the areola of the facet. α fp: such as α f for a proximal columnal. P: perilumen. Ontogeny of α stereom: from α fp to α s and α f.

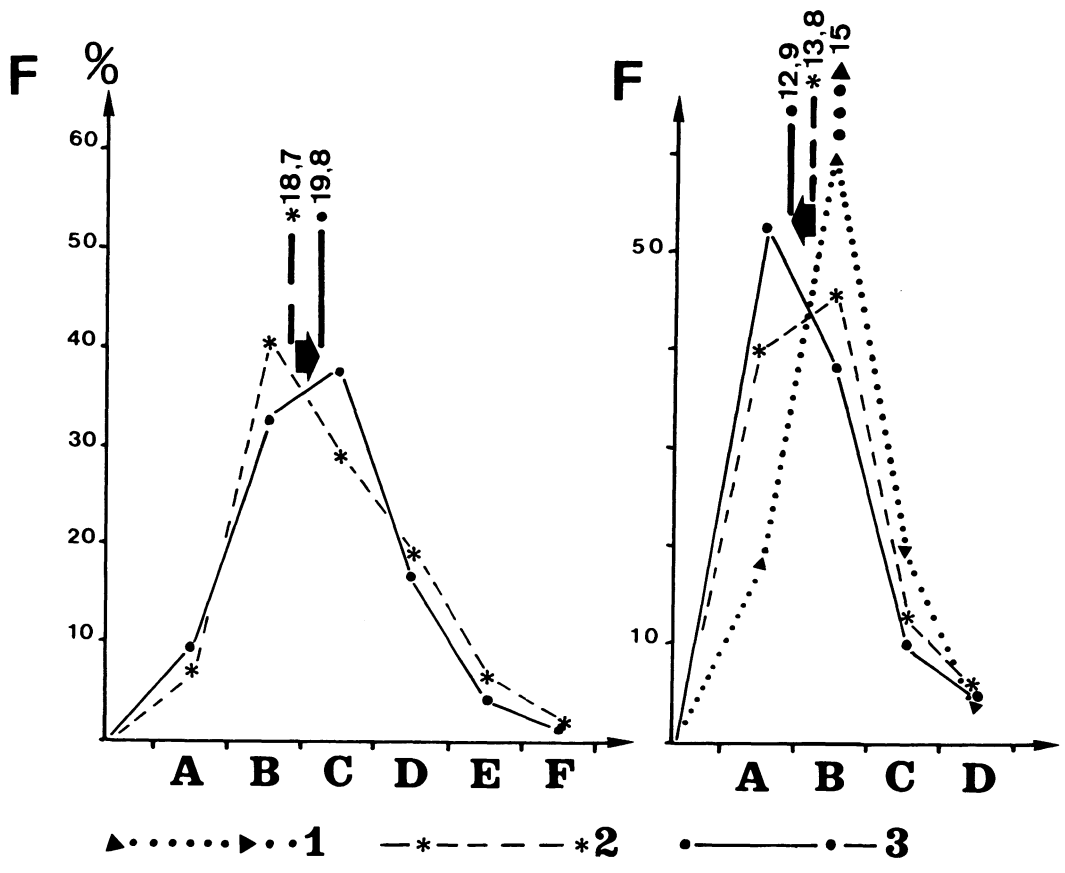

TEXT-FIG. 3 – Frequency histograms of the inner diameter of the α stereom meshes. At the left: *Diplocrinus maclearanus*; at the right: *D. (Annacrinus) wyville thomsoni*, 1: columnal of a young specimen; 2: proximal columnal of a mature specimen; 3: columnal of the distal half of the stem. A: less than 13 μ; B: between 13 μ and 18 μ; C: between 18 μ and 23 μ; D: between 23 μ and 28 μ; E: between 28 μ and 33 μ; F: more than 33 μ. The value of the average is pointed. For each histogram, 1500-1700 meshes are measured.

on the articulation; there are two depressions laterally into which the knobs on the corresponding surface on the nodal fit. Proximal cirrals are ovoid in cross section. The fulcral ridge is very short and there are two elevated triangular knobs on distal surfaces which present slippage between adjacent plates (Pl. 5, figs. 5, 6). Medial cirrals are more nearly circular; the dorsal ligament fossa is proportionately larger (Pl. 5, figs. 7, 8; Pl. 6, figs. 1, 2). The knobs and sockets which interlock adjacent cirrals are immediately lateral to and diagonally above the nerve canal which is 0.11 by 0.09 mm in diameter. Pore diameters range from 0.006 to 0.020 mm (Pl. 6, figs. 9, 10). On the most distal articulations (Pl. 6, fig. 5) the articular surface becomes flat (Pl. 6, fig. 8), bound together by the ligaments which penetrate the galleried stereom. The distal, terminal cirral has a dense surface on the exterior on the top and sides (Pl. 6, figs. 3, 4); the lower surface is flat and has a ridged pattern (Pl. 6, figs. 6, 7).

The cirral facet on the nodal of *Annacrinus wyvillethomsoni* (Pl. 13, figs. 9, 10; Pl. 14, fig. 6) is flatter than that of *D. maclearanus*. There are less conspicuous elevated triangular areas which fit into corresponding sockets on the proximal surface of the first oval cirral. The longest axis in the

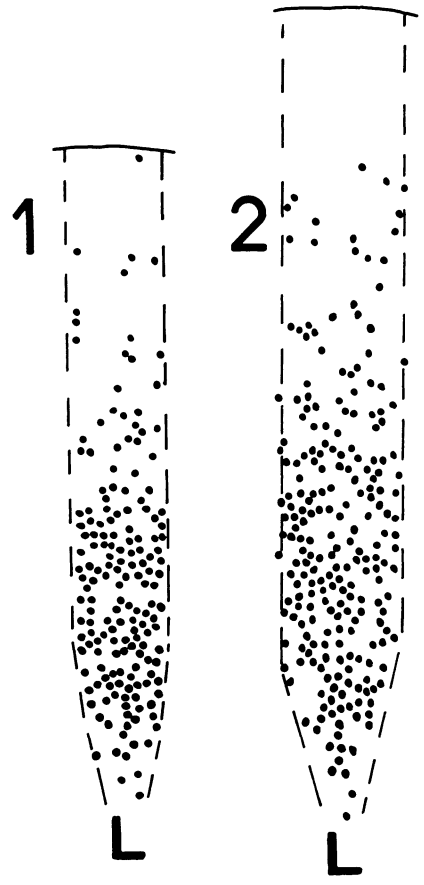

TEXT-FIG. 4 – *Diplocrinus maclearanus*: concentration of the mesh with the widest diameter in the inner half of the lanceolate areola. 1: proximal columnal; 2: distal columnal; L: lumen.

proximal cirrals is horizontal whereas in the medial cirrals it is vertical (Pl. 14, fig. 7). The distal surface of a medial cirral has two vertical raised areas immediately adjacent to the nerve canal (diameter 0.14 mm) and two depressions lateral to the raised areas (Pl. 14, figs. 2, 3). The proximal surface of a cirral has two corresponding concave and raised areas (Pl. 14, figs. 4, 5). Ligament pore diameters vary from 0.006 to 0.016 mm but are generally larger in the dorsal fossa. This would enhance the downward, contractive pull of the cirral. The external stereom of the cirral is much less porous. The exterior of the distalmost cirral is not as dense as *D. maclearanus* nor is the lower surface flat.

CONCLUSIONS

The crowns of *Diplocrinus maclearanus* and *Annacrinus wyvillethomsoni* are similar in size but the two species differ in their columns and cirri, apparently reflecting differences in life modes. *D. maclearanus* has a short stem with numerous long cirri which apparently is an adaptation to living on alcyonarians, sponges, or rocky substrates in areas of relatively high current velocities (Macurda and Meyer, 1976). The column of *A. wyvillethomsoni* is over twice as long, there are far fewer cirri, and

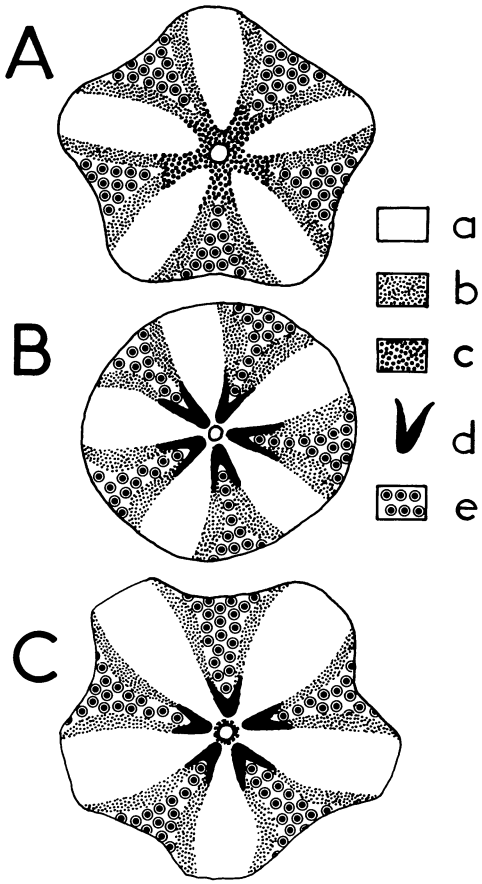

TEXT-FIG. 5 – Transversal cross section through distal columnals. A: *Diplocrinus alternicirrus*; B: *D.* (*Annacrinus*) *wyville thomsoni*; C: *Diplocrinus maclearanus*. a: α stereom (galleried); b: β stereom with middle wide meshes; c: thick calcitic β stereom with little meshes; d: calcitic thickness; e: β stereom with irregular large meshes.

they are much shorter. Roux (1975) has interpreted the form and growth of this column as an adaptation to muddy substrates, possibly in areas of high rates of sedimentation. There are skeletal differences in the basals and radials whose functional significance awaits studies of the soft tissues. The number of arms in *D. maclearanus* is fifty percent greater than in *A. wyvillethomsoni*. The overall length is similar however. The arms of *D. maclearanus* contain more lateral ligament fossa on some plates (as IBr_1) which allow greater bracing and stabilization of the arms which are recurved into the current when the animal is feeding (Macurda and Meyer, 1976). There are differences in the non-muscular arm articulations but there are apparently no significant differences in the form of the muscular or pinnular articulations. The elongate pinnulars would allow limited mobility between the pinnulars. Each crinoid would be capable of functioning as a rheophilic feeder.

Exclusive of the external morphology upon which A. H. Clark (1923) erected the genus *Annacrinus* the major aspects of the articulations of the cirri and the column are similar in both *D. maclearanus* and *A. wyvillethomsoni*. Nevertheless, differences in the form of the non-muscular arm articulations and lateral facets on the IBr_1 of *D. maclearanus* and the patterns of arm branching, plus the probable ecological adaptation of the species *A. wyvillethomsoni* with respect to the other species

of *Diplocrinus*, favors the retention of the taxa *Annacrinus*. Roux (1977) suggested a subgeneric level for *Annacrinus* and the generic level for *Diplocrinus*. The problem will be solved after a comparative study of all Caribbean isocrinids. It will then be possible to estimate the taxonomic significance of the skeletal morphology, based upon the means of characters and their variability.

The genus *Diplocrinus* is the only living isocrinid inhabiting both the Atlantic and the Indo-Pacific domains. It is probably, in spite of the apparent lack of comparable fossil forms, that this modern crinoid is an ancient taxon.

SPECIMEN LOCATIONS

Diplocrinus maclearanus
Collection: U.S. National Museum
Occurrence: Gerda Sta. 386, 27°09'N, 79°18'W, 604 m, Straits of Florida
Diplocrinus alternicirrus
Collection: British Museum (Nat. Hist.) Zoology
Occurrence: "Challenger expedition," st. 214 (Meangis Islands) syntype
D. (Annacrinus) wyvillethomsoni
Collection: Museum national d'Histoire naturelle – Paris Zoology, Echinoderms
Occurrence: "Thalassa" 1973, st. 452 (Bay of Biscay)

ACKNOWLEDGMENTS

Macurda wishes to thank W. Bigelow for access to the scanning electron microscopes in the Microprobe Laboratory, Department of Mechanical Engineering, University of Michigan. Procedures follow those given in Macurda and Meyer (1975). His research was supported by NSF grant GB-36439 and BMS 72-02486. Roux wishes to thank Mlle. Chapuis, Mmes. Guillaumin and Ragiudeau for SEM micrographs and B. H. Purser for translation of his part of the manuscript from French to English.

LITERATURE CITED

CLARK, A. H. 1923. A revision of the Recent representatives of the crinoid family Pentacrinidae with the diagnosis of two new genera. Jour. Wash. Acad. Sci., 13(1): 8-12.

DODERLEIN, L. 1907. Die gestielden Crinoiden der Siboga Expedition. Siboga Exped. Repts. 42a: 1-52.

MACURDA, D. B., JR. and D. L. MEYER. 1975. The microstructure of the crinoid endoskeleton. Univ. Kansas Paleon. Contrib., Paper 74: 1-18.

——and —— 1976. The identification and interpretation of stalked crinoids (Echinodermata) from deep-water photographs. Bull. Mar. Sci., 26: 205-215.

——, ——, and M. ROUX. 1978. The crinoid stereom. In R. C. Moore and C. Teichert (eds.), Treatise on Invertebrate Paleontology, Part T, Echinodermata 2, v.1, Geol. Soc. Am. and Univ. of Kansas, Lawrence: T217-228.

MEYER, D. L., C. MESSING, and D. B. MACURDA, JR. 1978. Zoogeography of tropical western Atlantic Crinoidea (Echinodermata). Bull. Mar. Sci., 28: 412-441.

ROUX, M. 1971. Recherches sur la microstructure des pédoncules de crinoides post Paleozoiques. Trav. Lab. Paleon. Orsay, France, 83 p.

—— 1974. Observations au microscope électronique à balayage de quelques articulation entre les ossicules du squellette des crinoïdes pédonculés actuels (Bathycrinidae et Isocrinina). Trav. Lab. Paleon. Orsay, France, 10p.

—— 1975. Microstructural analysis of the crinoid stem. Univ. Kansas Paleon. Contrib., Paper 75: 1-6.

—— 1976. Aspect de la variabilité et de la croissance au sein d'une population de la Pentacrine actuelle: *Annacrinus wyvillethomsoni*. Thallasia Jugoslavica, 12(1): 307-320.

—— 1977. The stalk joints of Recent Isocrinidae (Crinoidea). Bull. Brit. Mus. Nat. Hist. (Zool.) 32(3): 1-32.

EXPLANATION OF PLATE 1

Diplocrinus maclearanus (Wyville Thomson, 1877)

FIGS. 1, 6 – Views of theca and lower arms and complete individual respectively, x 1.0 and 0.5.
2, 3 – Stereo view of proximal surface of a basal; inner edge at top of photos, x 30.
4, 5 – Stereo view of top of radial; muscular facet faces left, x 30.
7, 8 – Stereo view of lower (right) and lateral (left) surfaces of radial, x 42.
9 – View of inner surface of basal, x 45.
10, 11 – Synostosial articulation on distal surface of IBr_1; ventral surface of plate in upper right, x 30.

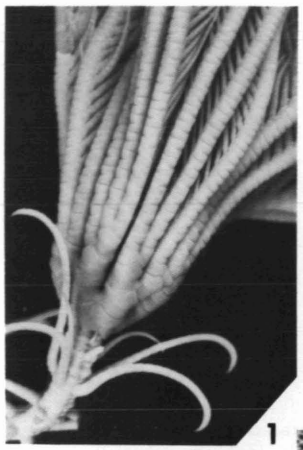
1

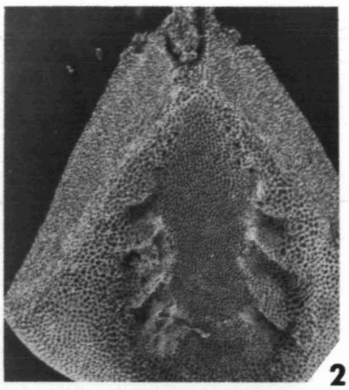
2

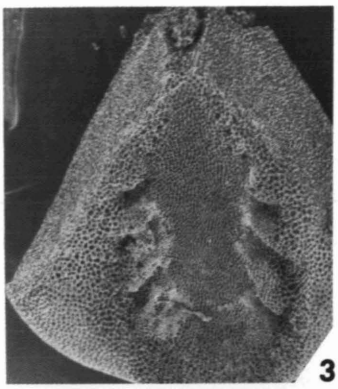
3

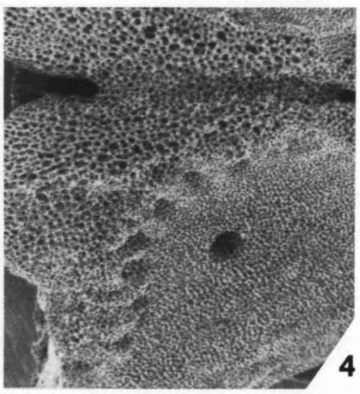
4

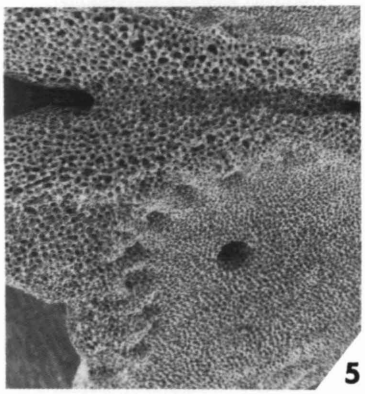
5

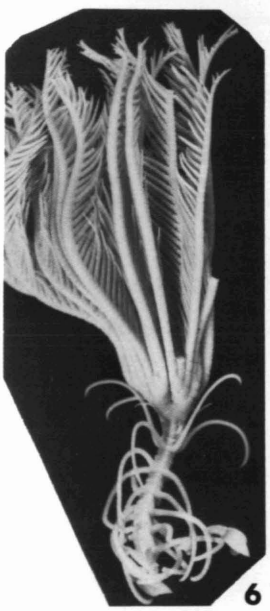
6

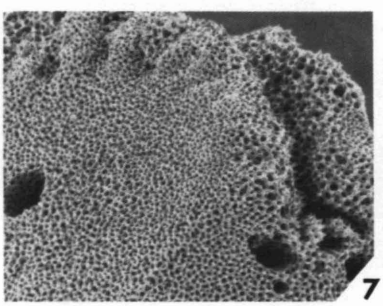
7

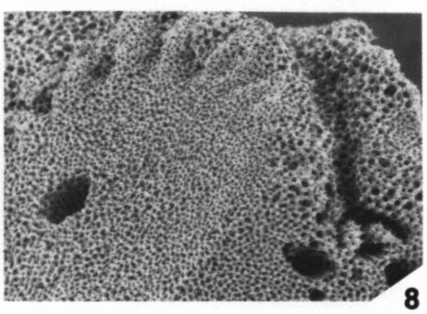
8

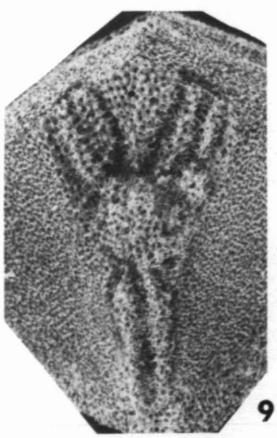
9

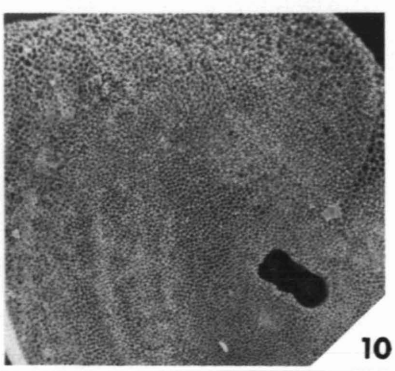
10

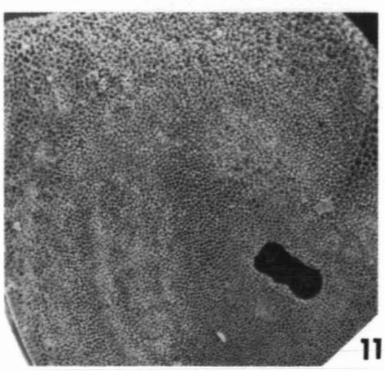
11

EXPLANATION OF PLATE 2

Diplocrinus maclearanus (Wyville Thomson, 1877)

FIG. 1 – Detail of stereom in ventral part of synostosial articulation between IBr_1 and IBr_2, x 270.

2, 3 – Stereo view of cryptosyzygial articulation on distal surface of $IIBr_1$; ventral surface to the right, x 30.

4 – Detail of stereom in dorsal part of synostosial articulation between IBr_1 and IBr_2, x 270.

5, 6 – Stereo view of cryptosyzygial articulation on proximal surface of $IIBr_2$; ventral surface at top, x 30.

7, 8 – Stereo view of detail of stereom on cryptosyzygial articulation on lateral edge of distal surface of $IIBr_1$, x 120.

9, 10 – Stereo view of axillary muscular articulations on distal surface of $IIBr_2$, x 30.

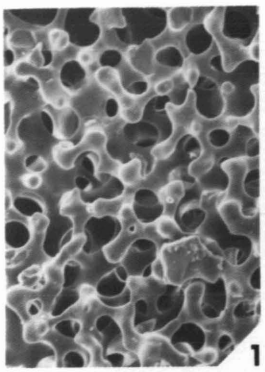
1

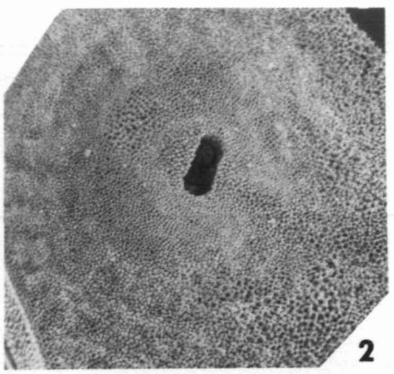
2

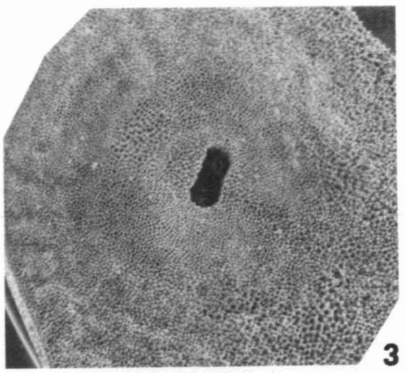
3

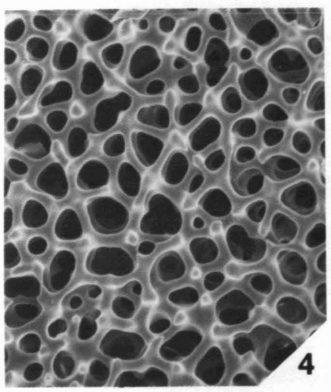
4

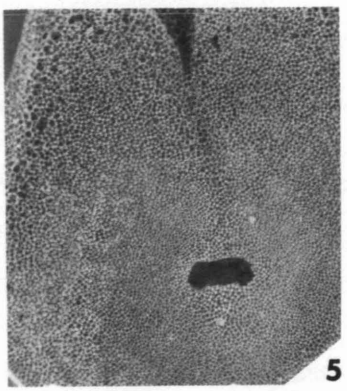
5

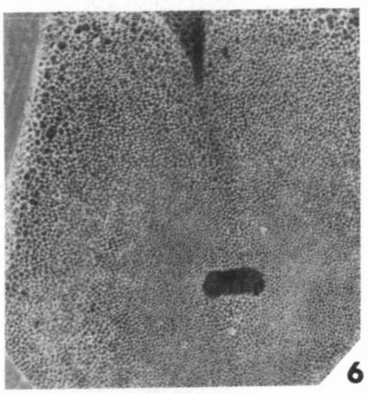
6

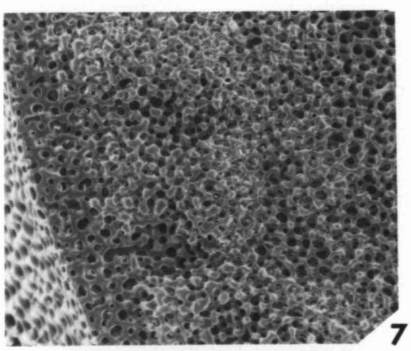
7

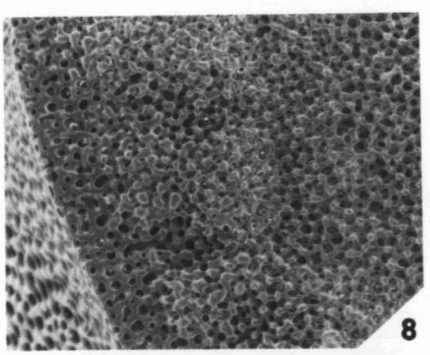
8

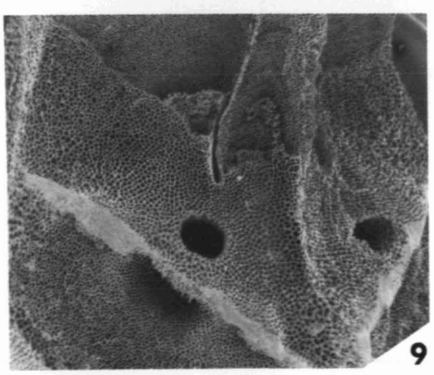
9

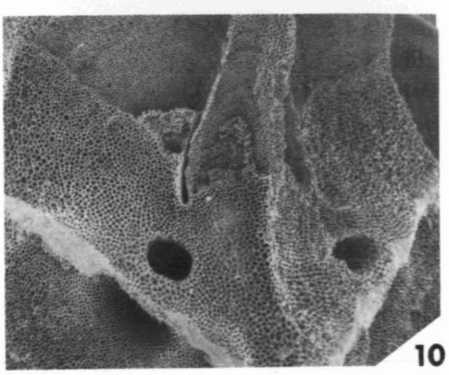
10

EXPLANATION OF PLATE 3

Diplocrinus maclearanus (Wyville Thomson, 1877)

FIGS. 1, 2 – Stereo view of detail of transition from ventral ligament to muscle fossa on distal surface of $IIBr_2$ (see Pl. 2, figs. 9, 10, left center), x 180.

3, 4 – Stereo view of proximal surface of Br_1, x 30.

5 – Detail of dorsal ligament fossa, proximal surface Br_1, x 600.

6, 7 – Stereo view of inner surface of Br_1, x 30.

8 – Detail of muscle fossa, proximal surface Br_1, x 600.

9, 10 – Stereo view of muscular articulation on proximal surface of a brachial, x 30.

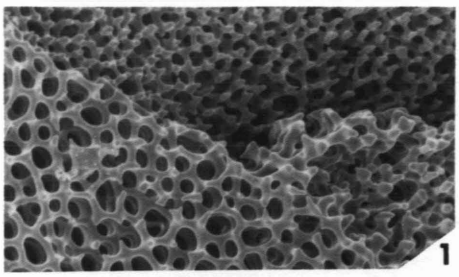
1

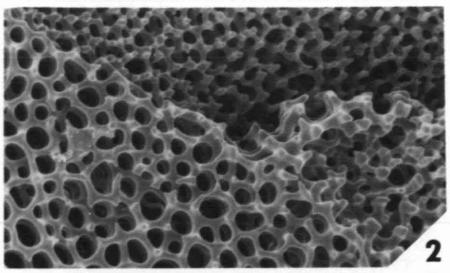
2

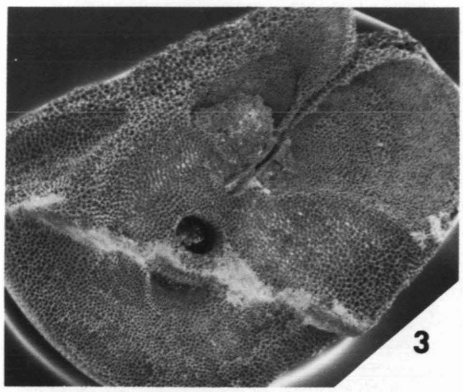
3

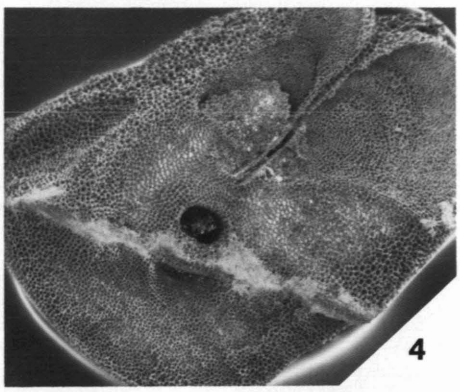
4

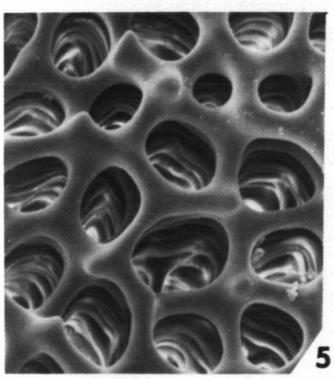
5

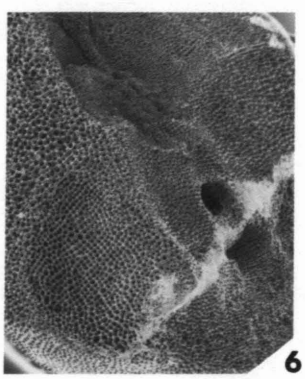
6

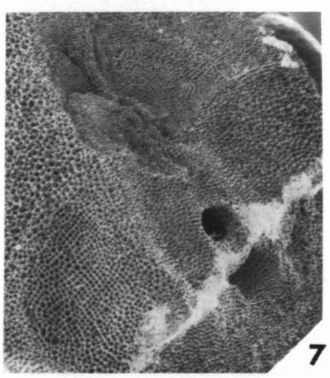
7

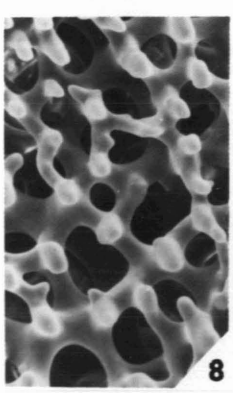
8

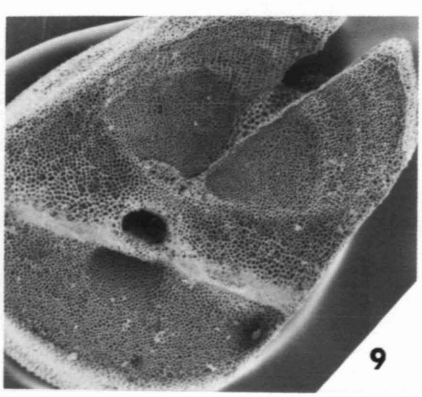
9

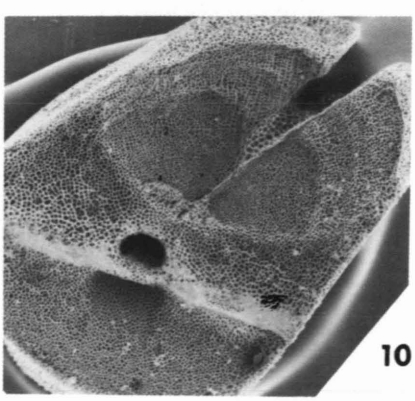
10

EXPLANATION OF PLATE 4

Diplocrinus maclearanus (Wyville Thomson, 1877)

FIGS. 1, 2 – Stereo view of a pinnular articulation on the upper (ventral) surface of a regular brachial; proximal direction to left, x 60.
3 – Lateral view of the exterior of a pinnular, x 78.
4, 5 – Stereo view of upper (ventral) surface of a pinnular, x 45.
6 – Muscular articulation on the surface of a distal pinnular, x 60.
7, 8 – Stereo view of muscular articulation on the distal surface of a medial pinnular, x 60.
9, 10 – Stereo view of muscular articulation on the proximal surface of a medial pinnular, x 60.

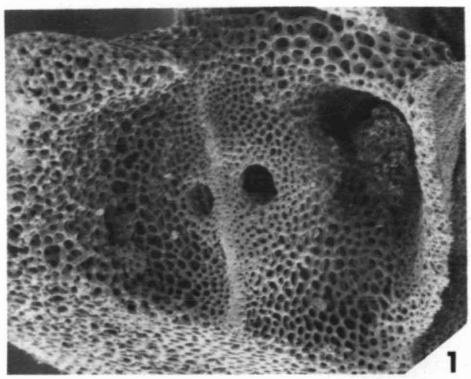
1

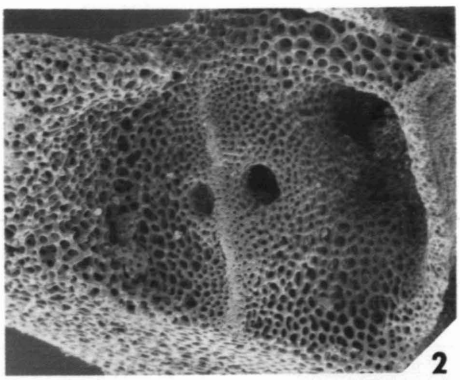
2

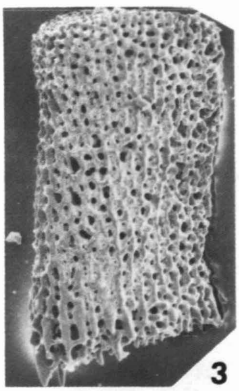
3

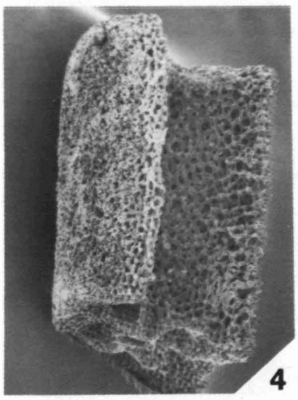
4

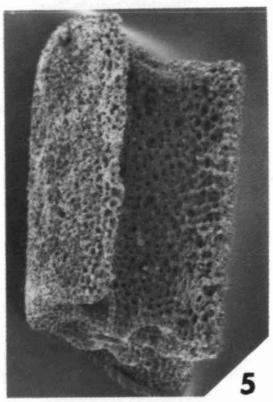
5

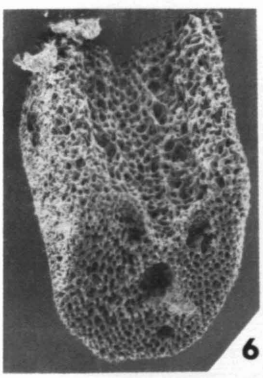
6

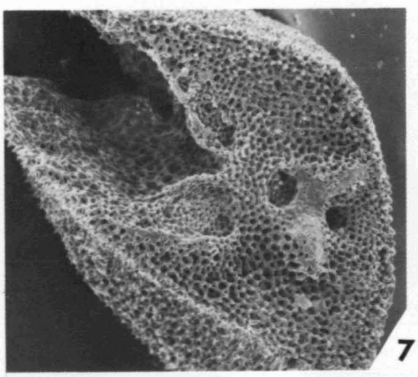
7

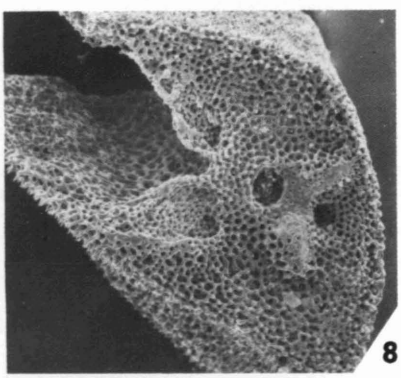
8

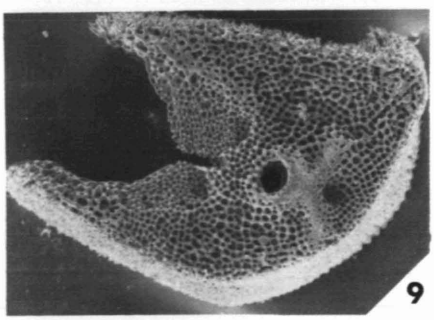
9

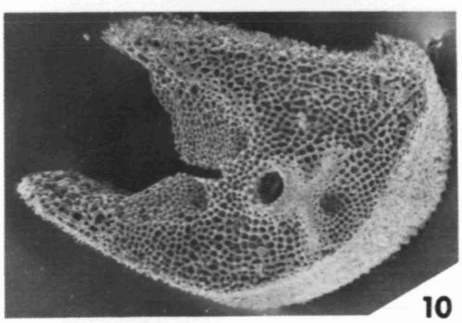
10

EXPLANATION OF PLATE 5

Diplocrinus maclearanus (Wyville Thomson, 1877)

FIGS. 1, 2 – Stereo view of cirral articulation on a nodal, x 33.
3, 4 – Stereo view of proximal surface of proximalmost cirral, x 36.
5, 6 – Stereo view of distal surface of a proximal cirral, x 36.
7, 8 – Stereo view of distal surface of a medial cirral, x 60.

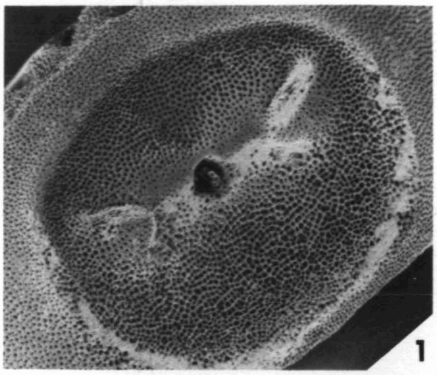
1

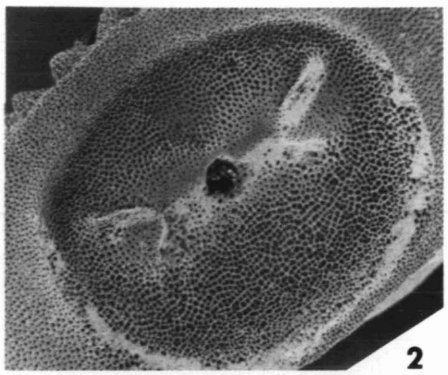
2

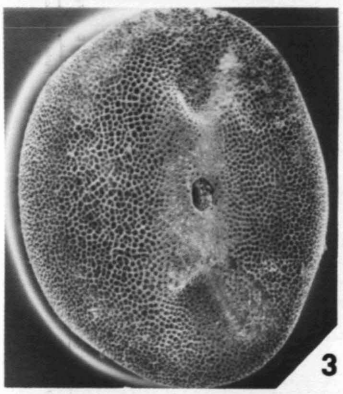
3

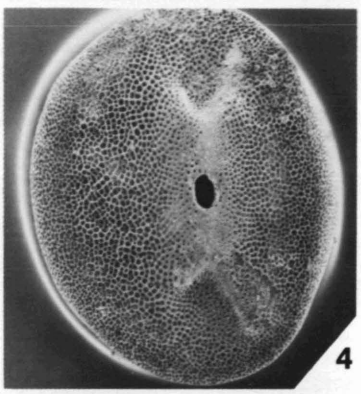
4

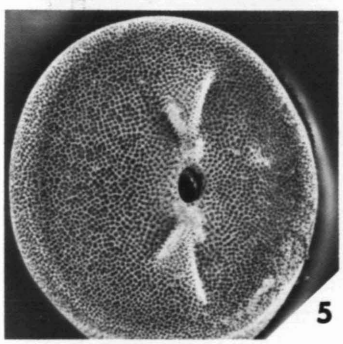
5

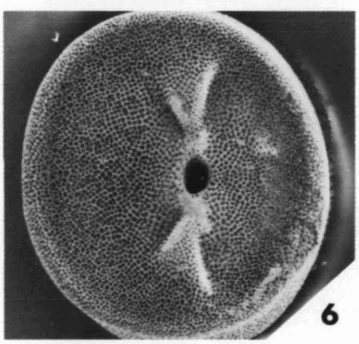
6

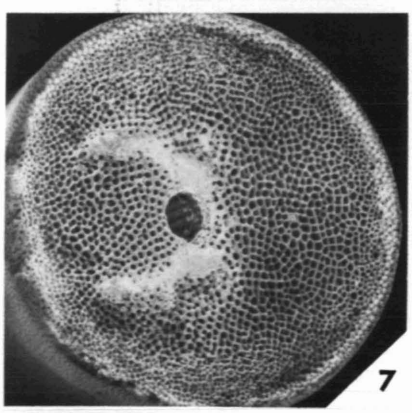
7

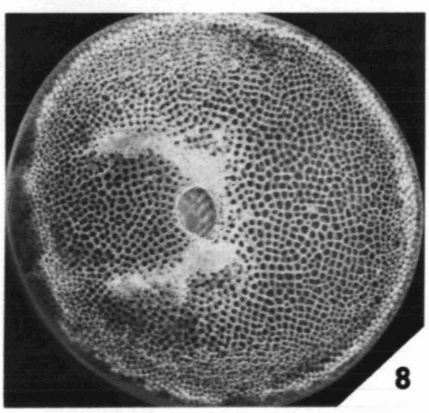
8

EXPLANATION OF PLATE 6

Diplocrinus maclearanus (Wyville Thomson, 1877)

FIGS. 1, 2 – Stereo view of proximal surface of a medial cirral, x 60.
3, 4 – Lateral stereo view of distalmost cirral, x 60.
5 – View of exterior of a cirral, x 60.
6, 7 – View of lower (dorsal) surface of distalmost cirral, x 120.
8 – View of articulation on proximal surface of distalmost articulation, x 90.
9 – View of alpha stereom of upper (ventral) part of a cirral facet, x 300.
10 – View of alpha stereo of lower (dorsal) part of a cirral facet, x 300.

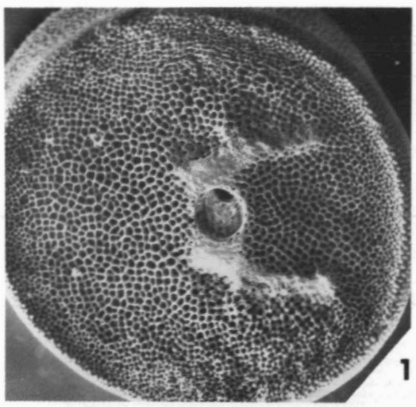
1

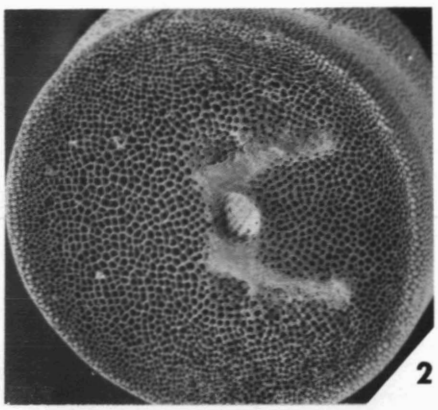
2

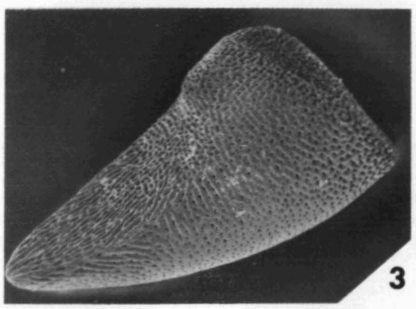
3

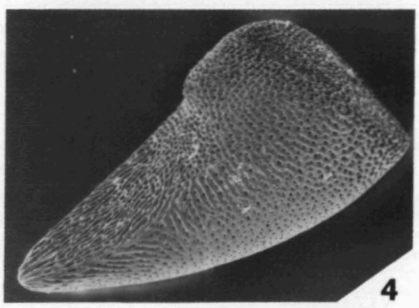
4

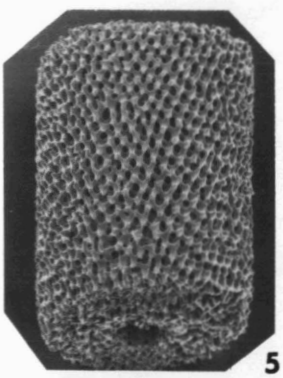
5

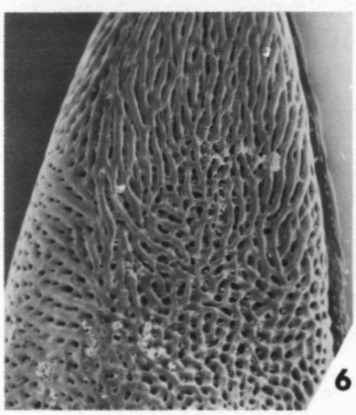
6

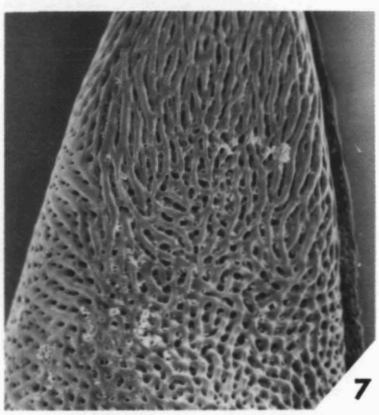
7

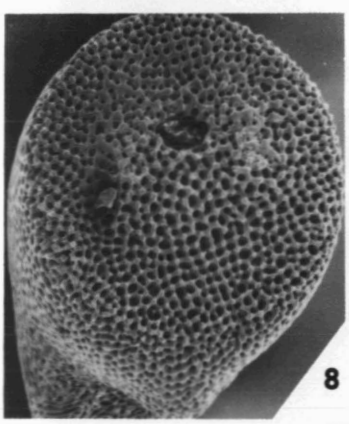
8

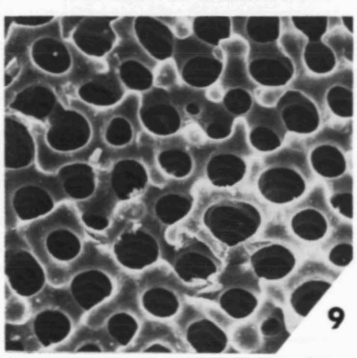
9

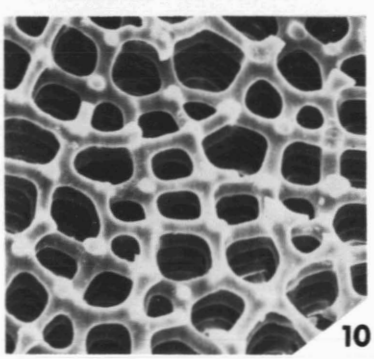
10

EXPLANATION OF PLATE 7

D. (Annacrinus) wyvillethomsoni (Wyville Thomson, 1872)

FIGS. 1, 8 – View of calyx and arms, and complete individual, x 1.5 and x 0.5.
2, 3 – Stereo view of uppermost columnals (left) and basals (right), x 18.
4, 5 – Stereo view of proximal surface of a basal, inner surface at top, x 24.
6, 7 – Stereo view of inner surface of a basal, x 42.
9, 10 – Stereo view of lower (lower right of picture) and lateral (upper part of picture) surface of two radials, x 18.

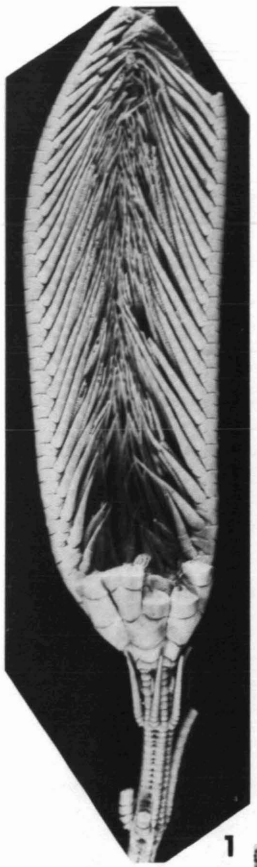

1

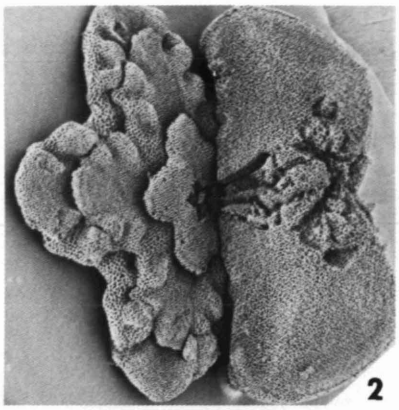

2

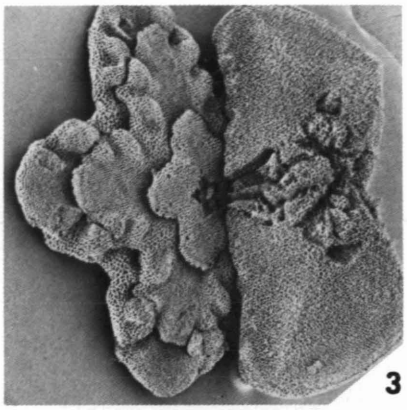

3

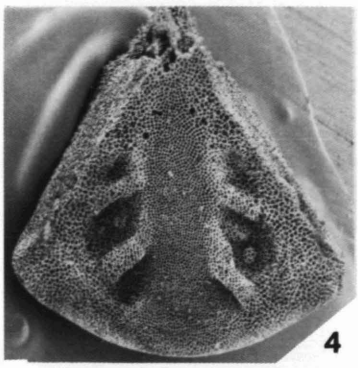

4

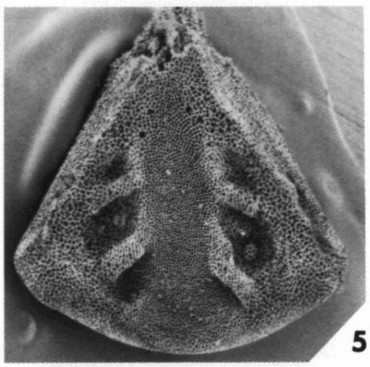

5

8

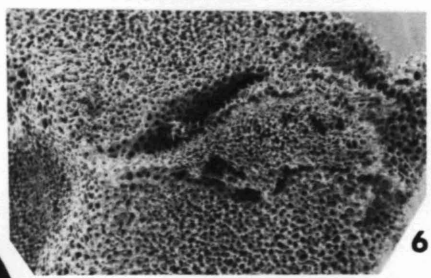

6

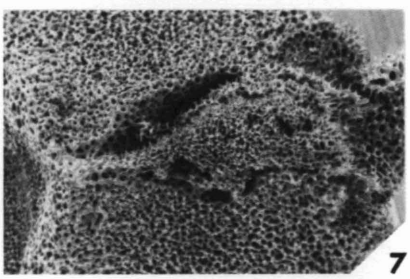

7

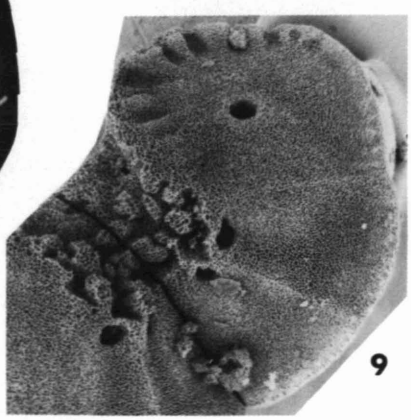

9

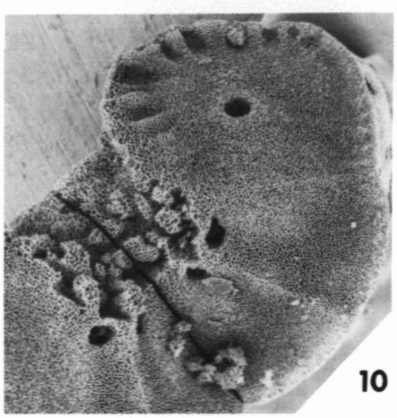

10

EXPLANATION OF PLATE 8

D. (*Annacrinus*) *wyvillethomsoni* (Wyville Thomson, 1872)

FIGS. 1, 2 – Stereo view of muscular articulation on a radial, x 18.
3, 4 – Stereo view of muscular articulation on proximal surface of IBr_1, x 15.
5, 6 – Stereo view of cryptosyzygial articulation on diatal surface of IBr_1, x 15.
7 – Ventral view (upper surface) of IBr_1, proximal surface to right, x 15.
8, 9 – Stereo view of cryptosyzygial articulation on proximal surface of IBr_2, x 15.

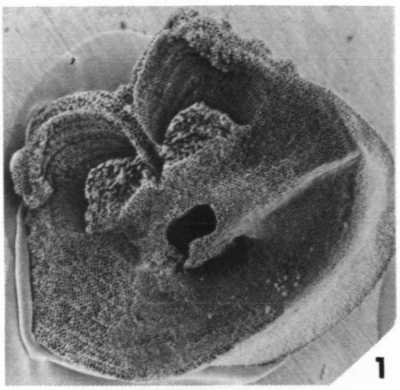
1

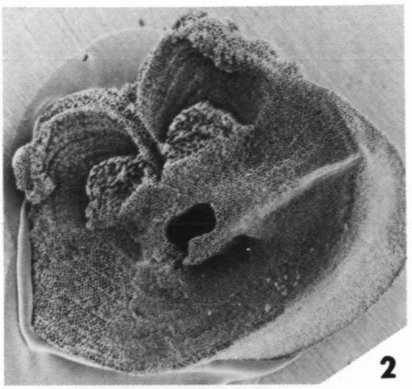
2

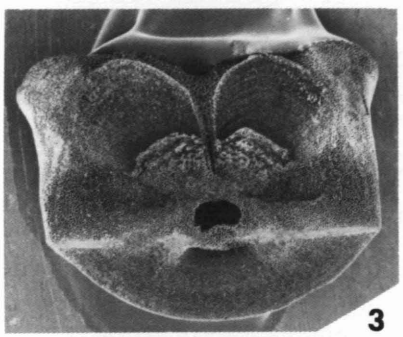
3

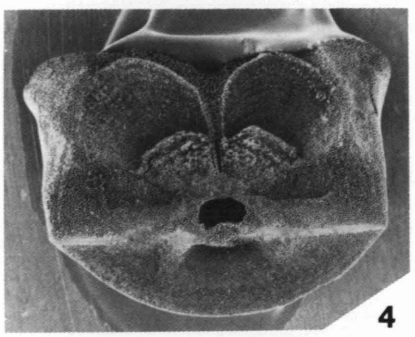
4

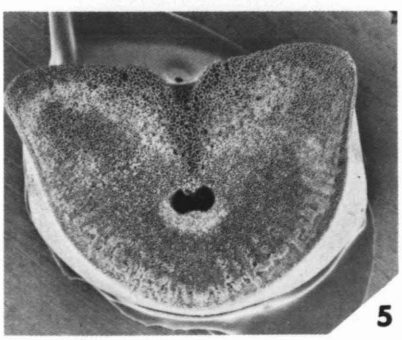
5

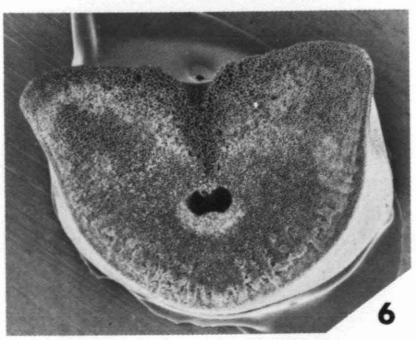
6

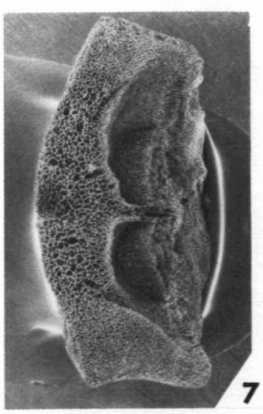
7

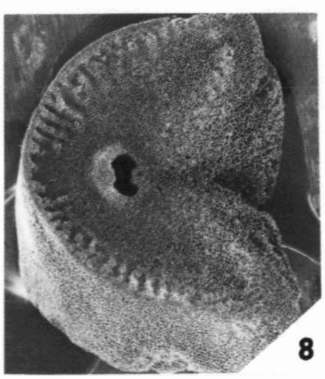
8

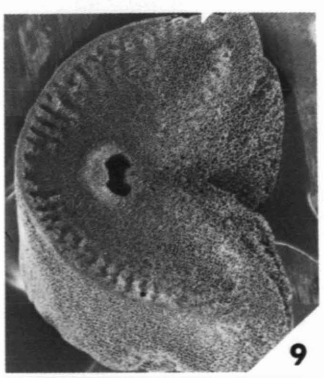
9

EXPLANATION OF PLATE 9

D. (*Annacrinus*) *wyvillethomsoni* (Wyville Thomson, 1872)

FIG. 1 – Lateral view of $IIBr_1$, proximal surface on left, x 15.
2, 3 – Stereo view of axillary muscular articulations on distal surface of IBr_2, x 15.
4 – View of asymmetric muscular articulation on proximal surface of Br_1, x 15.
5, 6 – Stereo view of muscular articulation on proximal surface of $IIBr_1$, x 15.
7 – View of cryptosyzygial articulation on proximal surface of Br_2, x 15.
8, 9 – Stereo view of cryptosyzygial articulation on distal surface of $IIBr_1$, x 15.
10 – View of upper (ventral) surface of $IIBr_2$; proximal surface to the right, x 15.
11, 12 – Stereo view of axillary muscular articulation distal surface of $IIBr_2$, x 15.

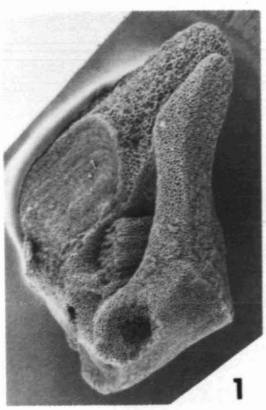
1

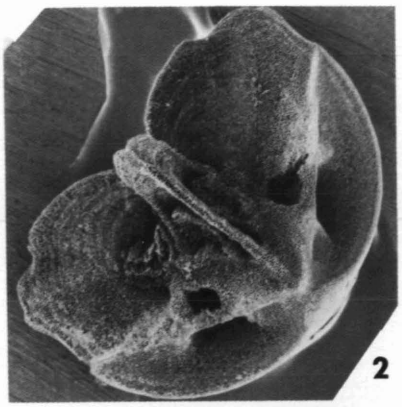
2

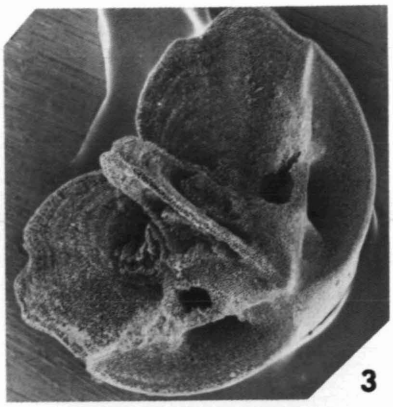
3

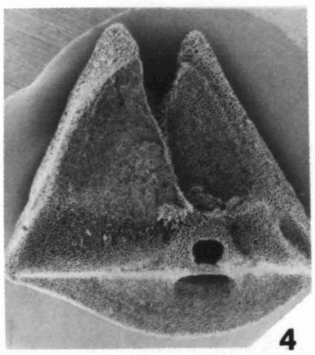
4

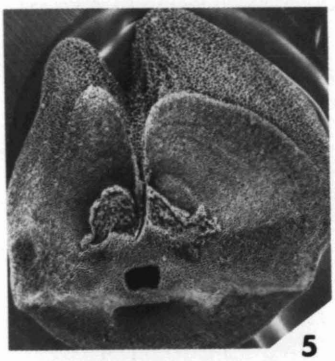
5

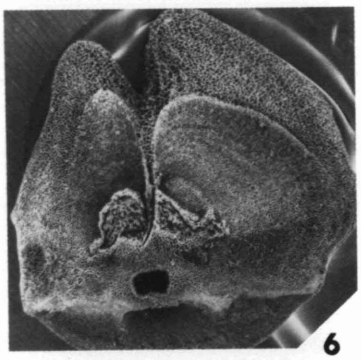
6

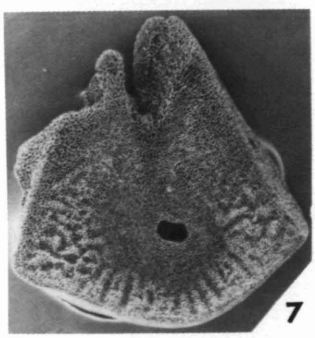
7

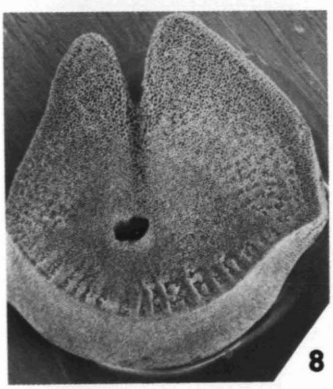
8

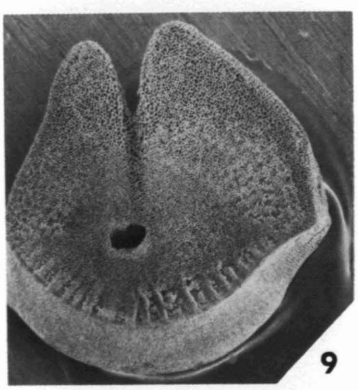
9

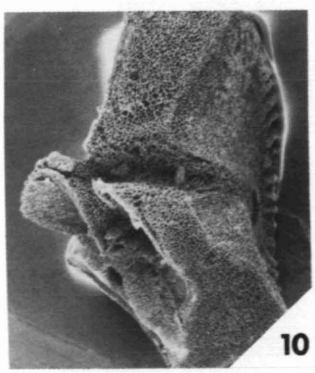
10

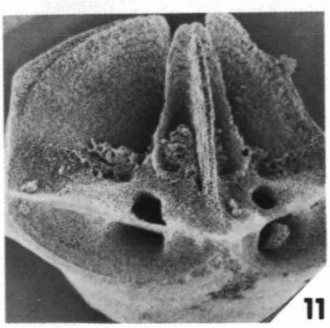
11

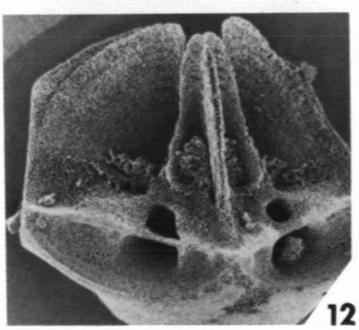
12

EXPLANATION OF PLATE 10

D. (Annacrinus) wyvillethomsoni (Wyville Thomson, 1872)

FIGS. 1, 2 – Stereo view of muscular articulation on proximal surface of medial brachial, x 24.
3, 4 – Stereo view of muscular articulation on distal surface of medial brachial, x 24.
5, 6 – Stereo view of upper (ventral) surface of a medial brachial, x 24.
7 – Lateral view of a medial brachial, x 24.
8, 9 – Stereo view of transition from the ventral ligament fossa (upper part of picture) to muscle fossa (lowest part of picture) on proximal surface a medial brachial, x 120.

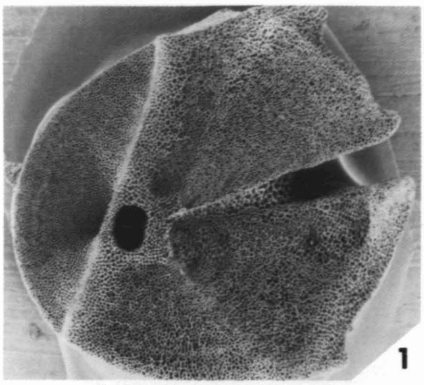
1

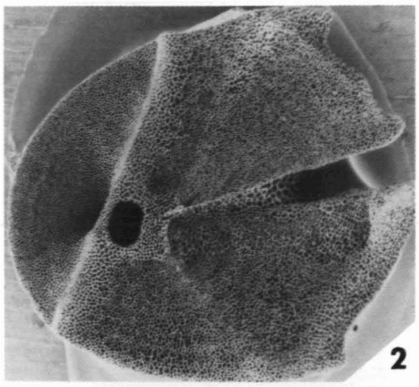
2

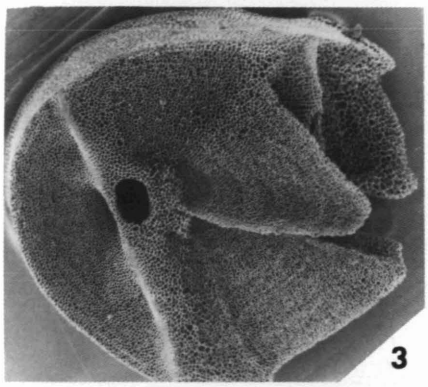
3

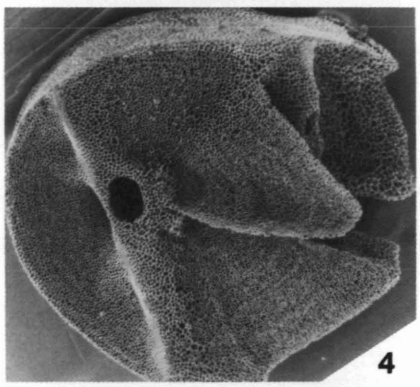
4

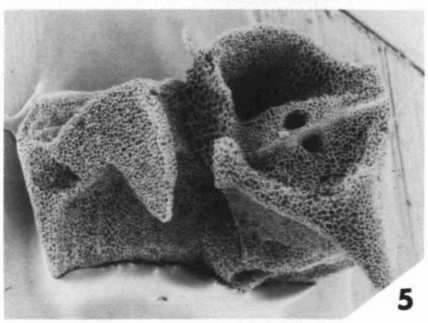
5

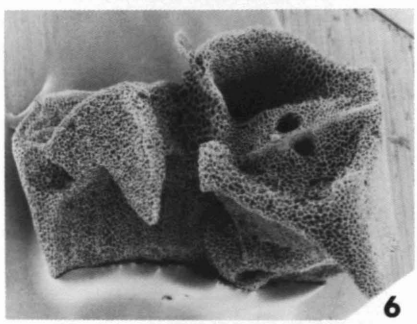
6

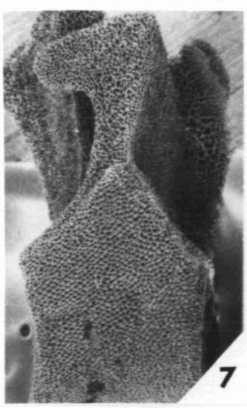
7

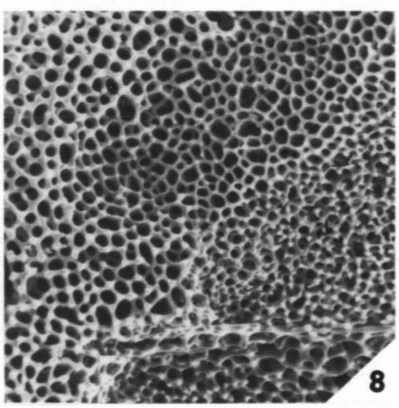
8

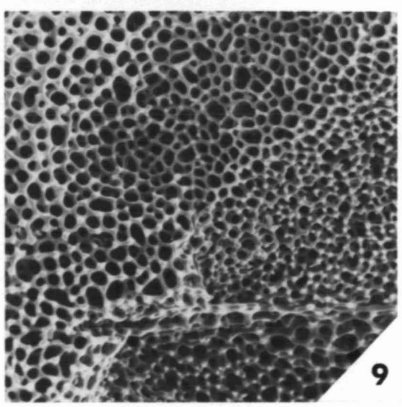
9

EXPLANATION OF PLATE 11

D. (*Annacrinus*) *wyvillethomsoni* (Wyville Thomson, 1872)

FIGS. 1, 2 – Stereo view of muscular articulation on distal surface of a distal brachial, x 48.

3, 4 – Stereo view of muscular articulation on proximal surface of a distal brachial, x 48.

5, 6 – Stereo view of pinnular articulation on upper (ventral) surface of Br_2, x 100.

7, 8 – Stereo view of pinnular articulation on upper (ventral) surface of a distal brachial, x 84.

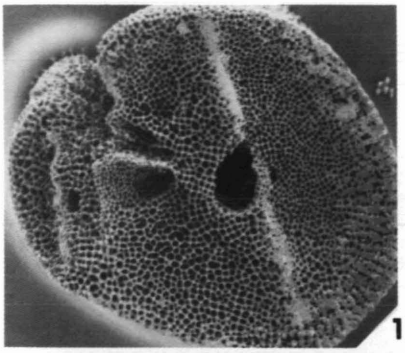
1

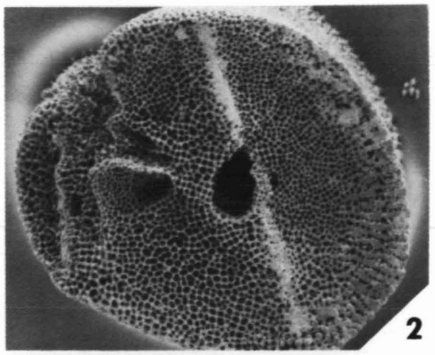
2

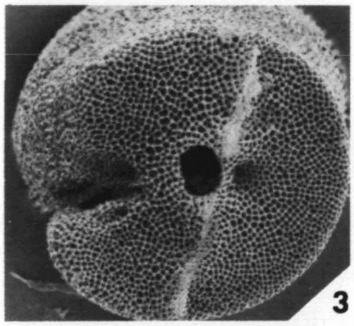
3

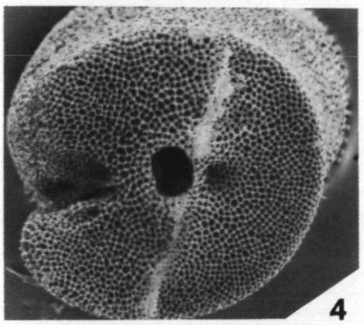
4

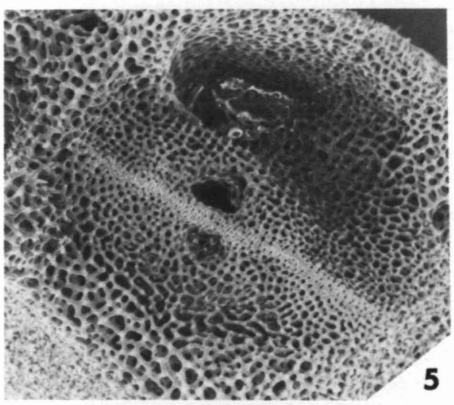
5

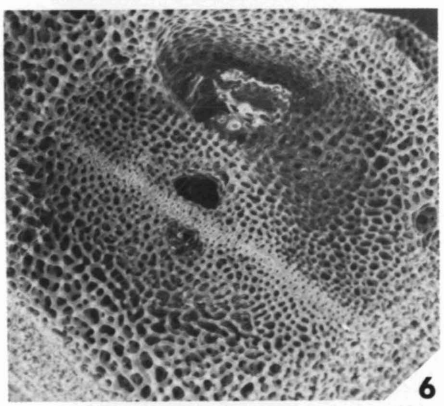
6

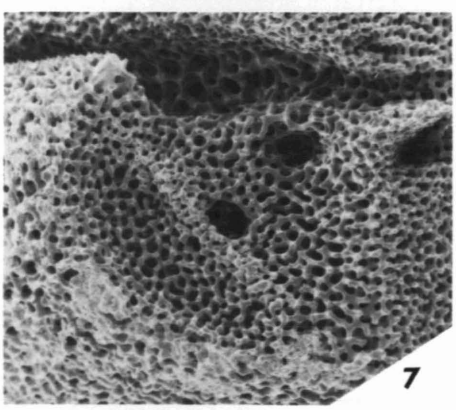
7

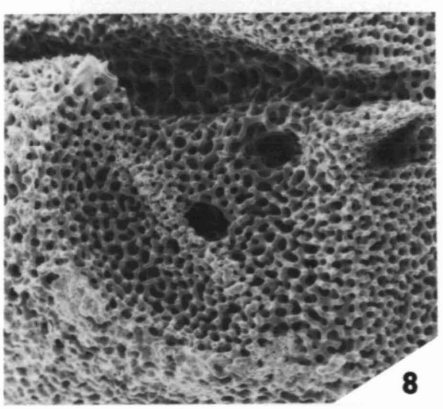
8

EXPLANATION OF PLATE 12

D. (*Annacrinus*) *wyvillethomsoni* (Wyville Thomson, 1872)

FIG. 1 – Proximal surface of P_1 of oral pinnule, x 42.
2, 3 – Stereo view of proximal surface of P_1 of medial pinnule, x 42.
4 – Distal surface of P_1 of oral pinnule, x 42.
5, 6 – Stereo view of surface of P_1 of medial pinnule, x 42.
7, 8 – Stereo view of upper (ventral) surface of P_1 of oral pinnule; proximal surface at base of picture, x 42.
9 – Proximal surface of P_2 of medial pinnule, x 42.
10 – Proximal surface of P_2 of oral pinnule, x 42.
11, 13 – Stereo view of distal surface of P_2 of oral pinnule, x 42.
12 – View of upper (ventral surface) of P_2 of oral pinnule; proximal surface at bottom of picture, x 42.

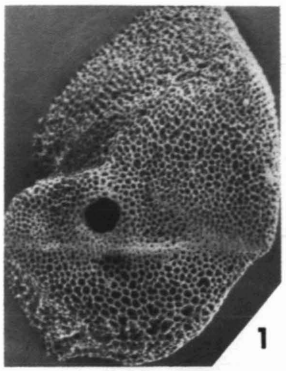
1

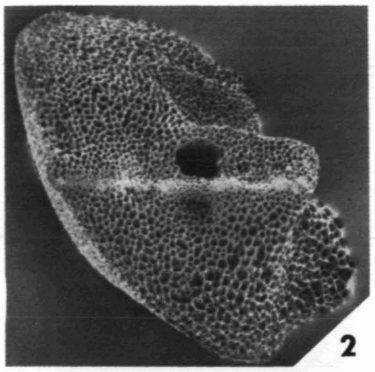
2

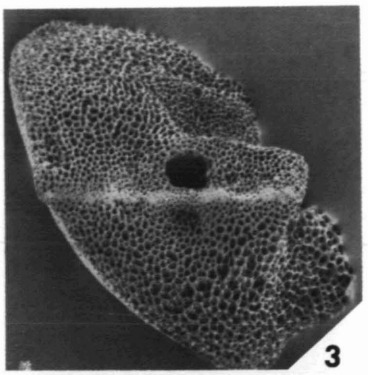
3

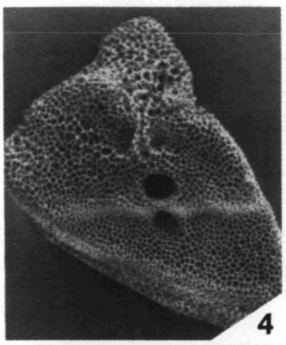
4

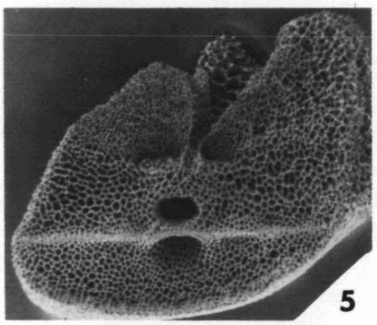
5

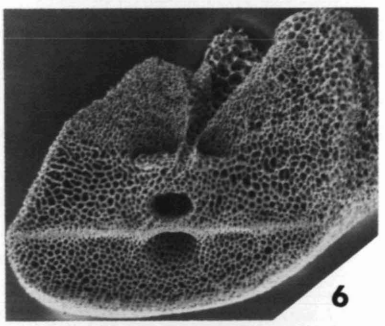
6

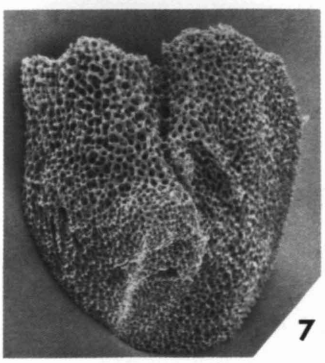
7

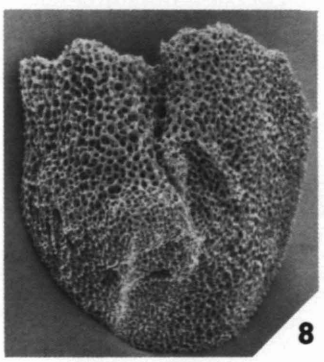
8

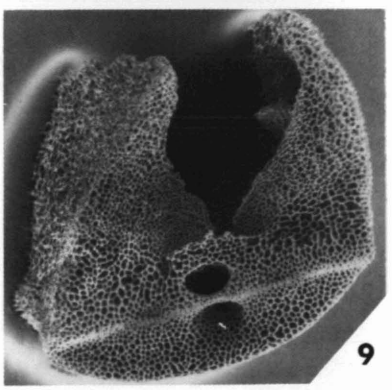
9

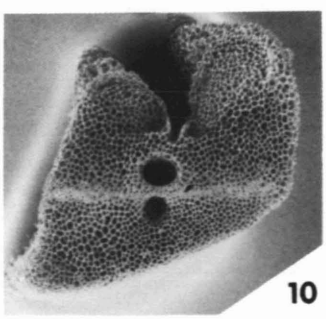
10

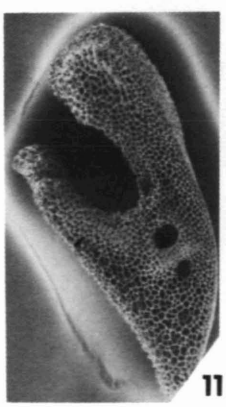
11

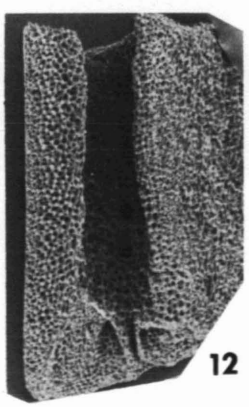
12

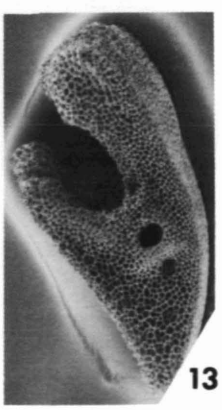
13

EXPLANATION OF PLATE 13

D. (*Annacrinus*) *wyvillethomsoni* (Wyville Thomson, 1872)

FIG. 1 – Proximal surface of a distal pinnular from a medial pinnule, x 90.
2, 3 – Stereo view of distal surface of a medial pinnular from a medial pinnule, x 66.
4 – Proximal surface of proximalmost cirral, x 30.
5, 6 – Stereo view of proximal surface of a medial pinnular from a medial pinnule, x 66.
7, 8 – Inclined distal stereo view of a distal pinnular, x 60.
9, 10 – Stereo view of cirral facet on nodal, x 30.

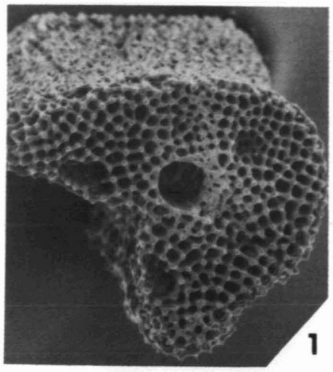
1

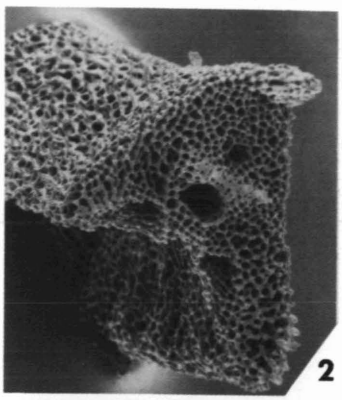
2

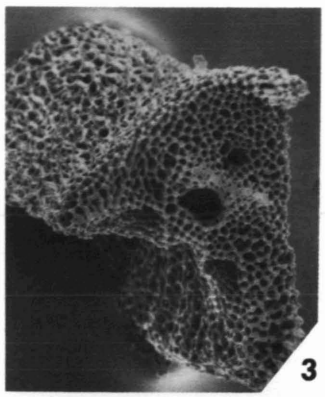
3

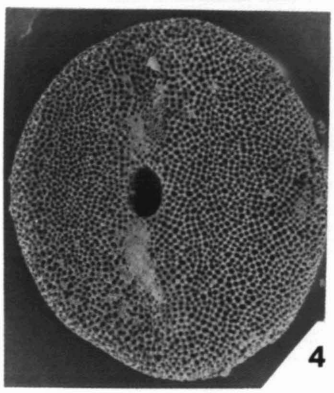
4

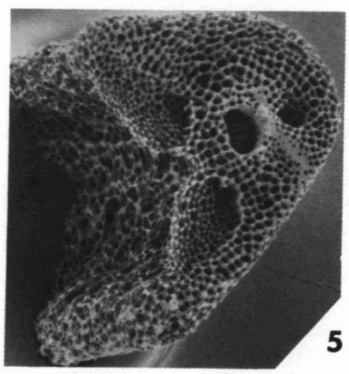
5

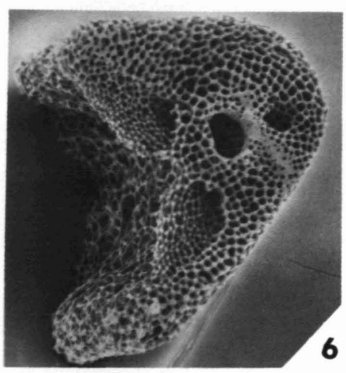
6

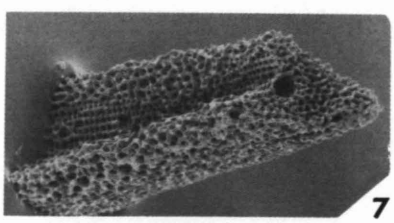
7

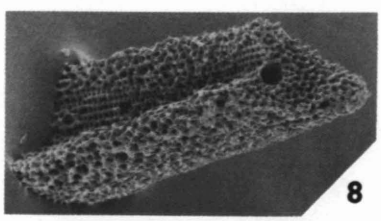
8

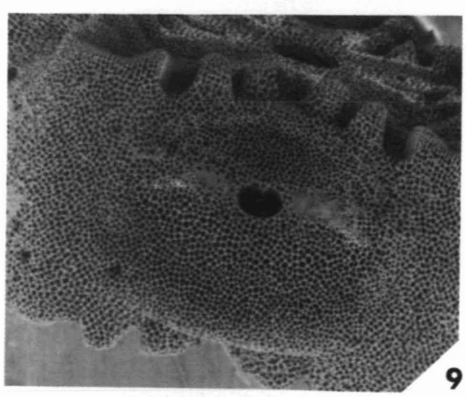
9

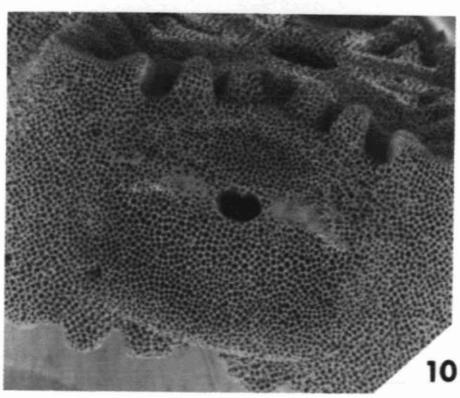
10

EXPLANATION OF PLATE 14

D. (*Annacrinus*) *wyvillethomsoni* (Wyville Thomson, 1872)
unless otherwise indicated

FIG. 1 – Lateral view of distalmost cirral, x 60.
2, 3 – Stereo view of distal surface of a medial cirral, x 30.
4, 5 – Stereo view of proximal surface of a medial cirral, x 30.
6 – Lateral view of a nodal showing the proximal part of a cirrus and the cirral socket, x 15.
7 – Lateral view of a medial cirral, x 30.
8 – *Diplocrinus maclearanus* (Wyville Thomson, 1877). Transverse cross section of a columnal showing at the right the thickened calcite at the edge of the lumen, and the inner part of the crenularium at the left, x 100.
9 – *Diplocrinus alternicirrus* (Carpenter, 1884). Transverse cross section of a columnal, x 60.

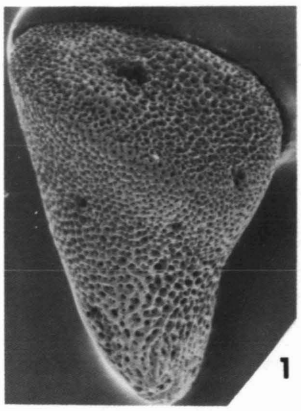
1

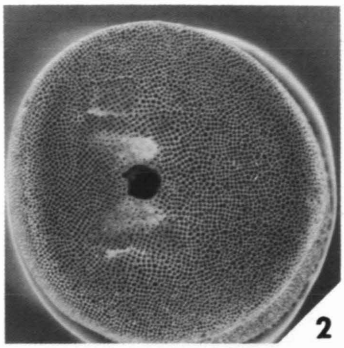
2

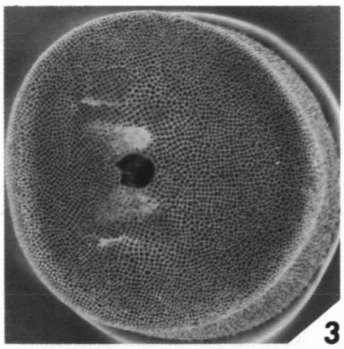
3

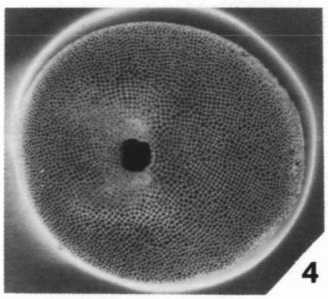
4

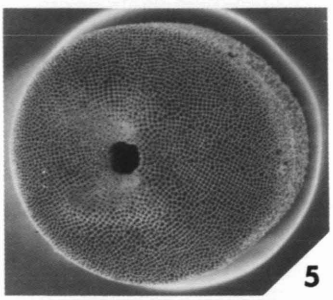
5

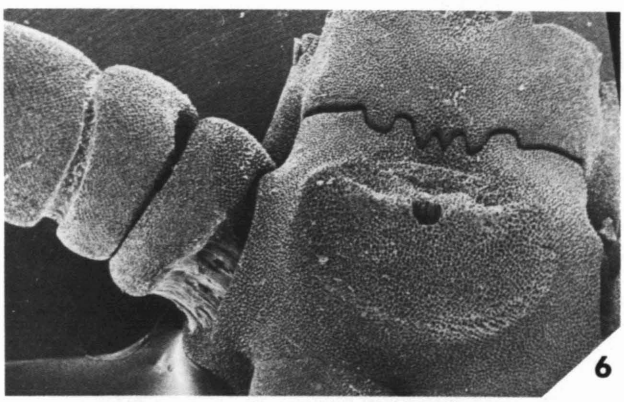
6

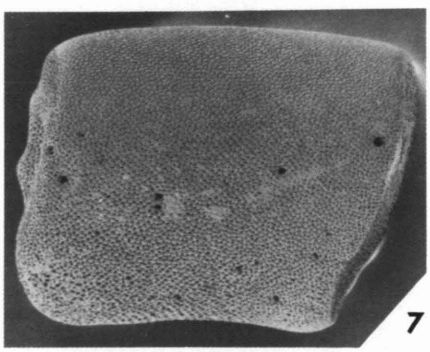
7

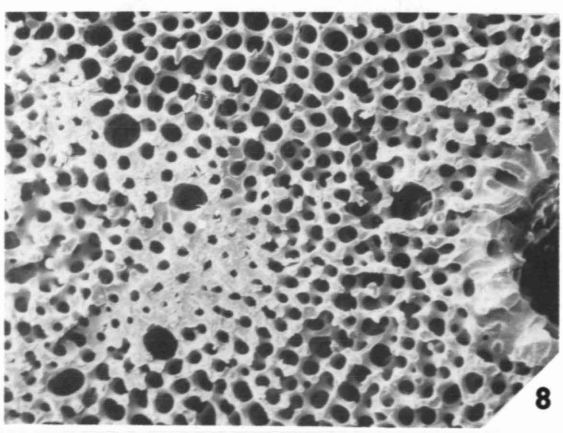
8

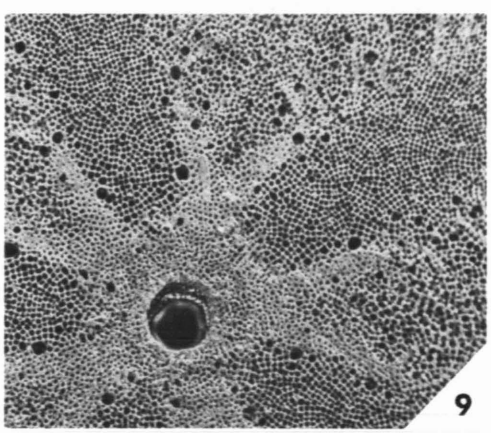
9

EXPLANATION OF PLATE 15

FIG. 1 – *Diplocrinus maclearanus*, lateral view of a nodal with a cirrus socket, x 15.

2 – The same nodal, detailed lateral view of the crenularium of the proximal symplexy, x 80.

3 – The same nodal, proximal symplexy, x 20.

4-7 – *Diplocrinus maclearanus*, several aspects of symplexial facets, x 14.

8 – *Diplocrinus maclearanus*, the upper proximal columnal without crenularium, x 50.

9 – The same specimen, facet of a proximal internodale showing an interpetaloid groove and the first stage of the crenularium development, x 40.

10 – The same specimen, adjacent internodal facet of the same articulation, x 40.

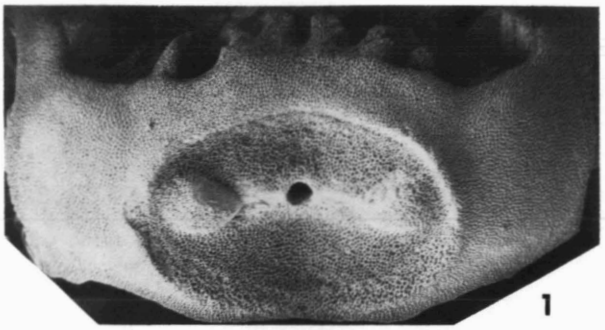

1

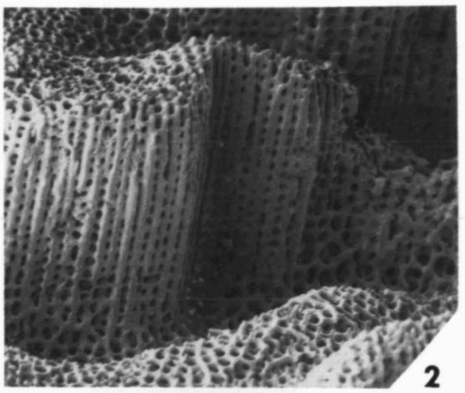

2

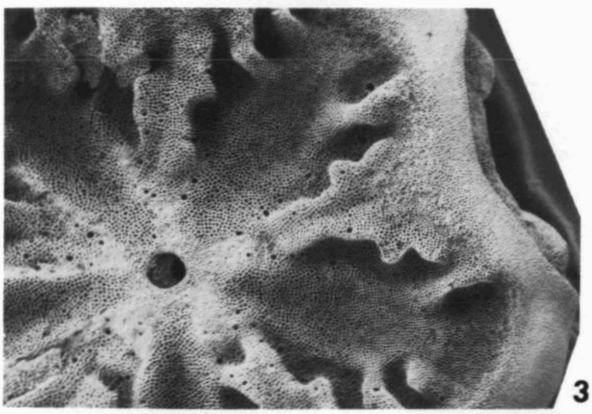

3

4

5

6

7

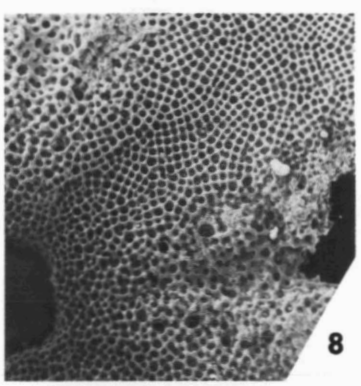

8

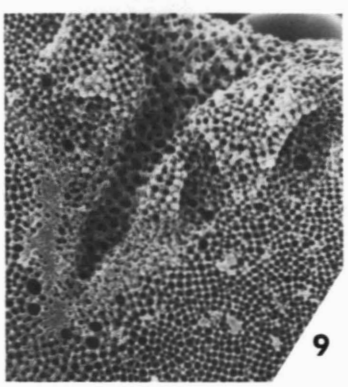

9

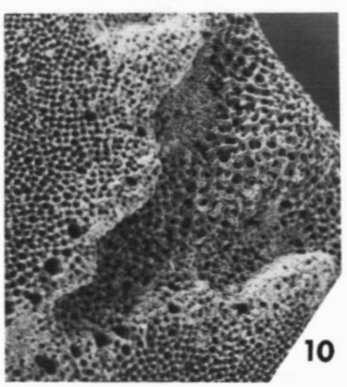

10

EXPLANATION OF PLATE 16

FIG. 1 – *Diplocrinus maclearanus*, distal synostosis of a nodal, see the symmorphy of the left interpetaloid zone, x 15.
2 – The same facet showing the low microstructural differentiation of the interpetaloid zones, x 20.
3 – The same facet, spicules filling in the axial canal, x 200.
4 – The same facet, syzygial stereom of the external part of an interpetaloid zone, x 100.
5 – *Diplocrinus alternicirrus*, distal synostosis of a nodal, see the regular symmorphy of the interpetaloid zones, x 10.
6 – *Diplocrinus alternicirrus*, symplexy, x 15.
7 – *Annacrinus wyvillethomsoni*, distal synostosis of a nodal, x 15.
8 – The same facet, crenularium, x 60.
9 – Synostosis of the adjacent internodal, crenularium, x 60.
10 – Detail of the fig. 8, x 120.
11 – The facet of the fig. 9, stereom filling in the axial canal, x 150.
12 – The facet of the fig. 8, axial canal, inner stereom filling in the secondary lumen, x 300.

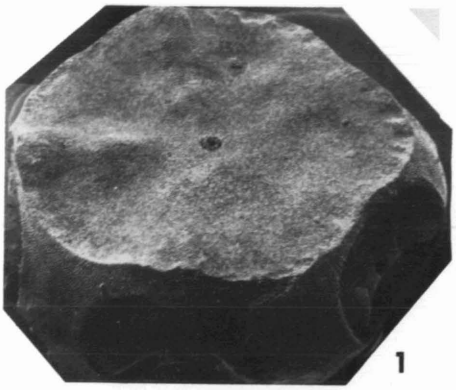
1

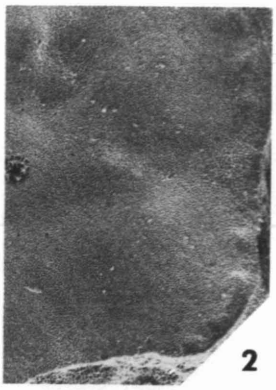
2

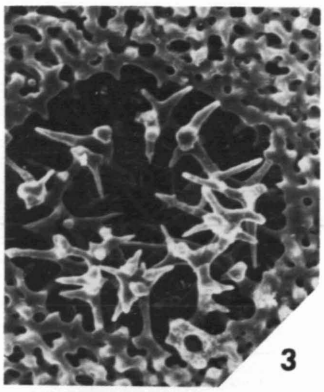
3

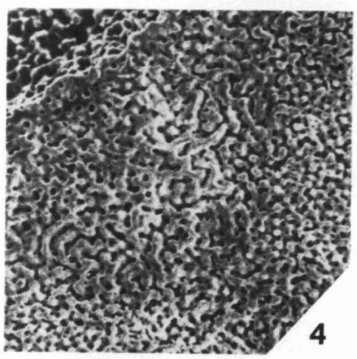
4

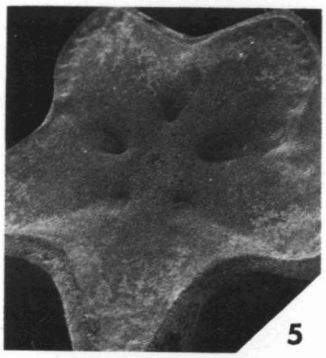
5

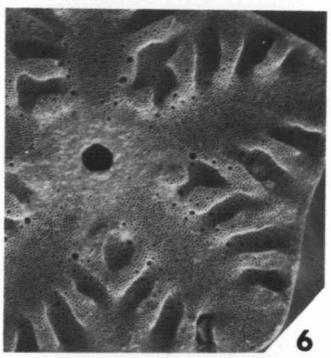
6

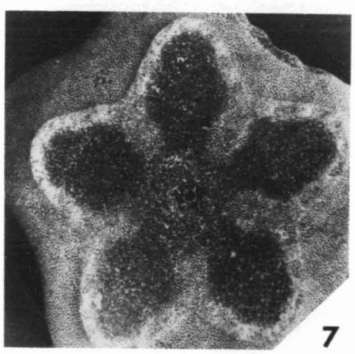
7

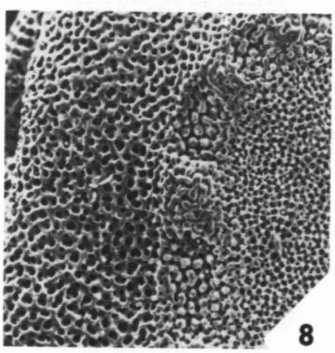
8

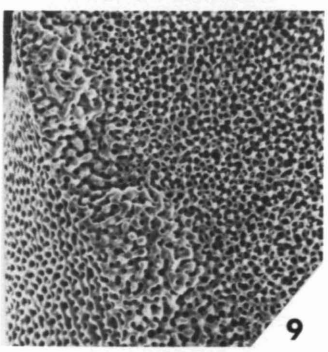
9

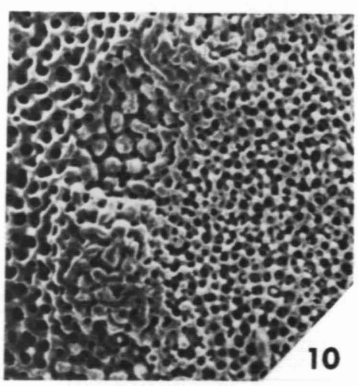
10

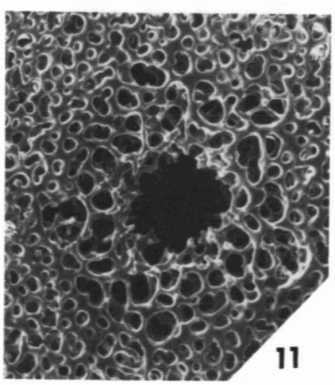
11

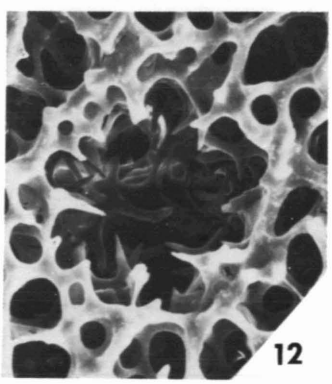
12

EXPLANATION OF PLATE 17

FIG. 1 – *Annacrinus wyvillethomsoni*, upper proximal part of the stem, a new columnal appears inducted by the stereom of the oldest one. See the synostosial stereom of the interpetaloid zone, x 30.

2 – Detail of the same joint, the new crenularium (at the left) is inducted by the oldest one (at the right), x 200.

3 – *Annacrinus wyvillethomsoni*, symplexy, the most frequent morphology of an internodal articulation, x 25.

4 – Detail of the regular crenularium of the same symplexy, x 40.

5 – *Annacrinus wyvillethomsoni*, proximal symplexy of an old distal nodal, x 20.

6 – *Annacrinus wyvillethomsoni*, ankylosed symplexy of a distal internodal, x 20.

7 – *Annacrinus wyvillethomsoni*, transverse cross section of a young distal columnal, x 40.

8 – *Diplocrinus macleranus*, proximal part of a pinnule, x 12.

9 – Distal part of the same pinnule, x 12.

10 – Detail of the fig. 8, x 30.

11 – Distal part of the same pinnule, x 30.

12 – *Annacrinus wyvillethomsoni*, ventral face of a pinnule, x 30.

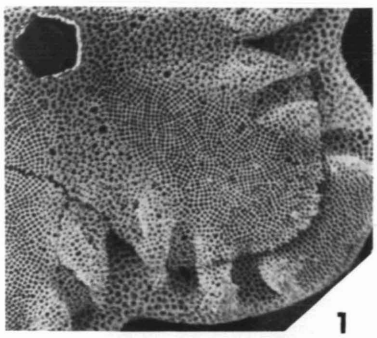
1

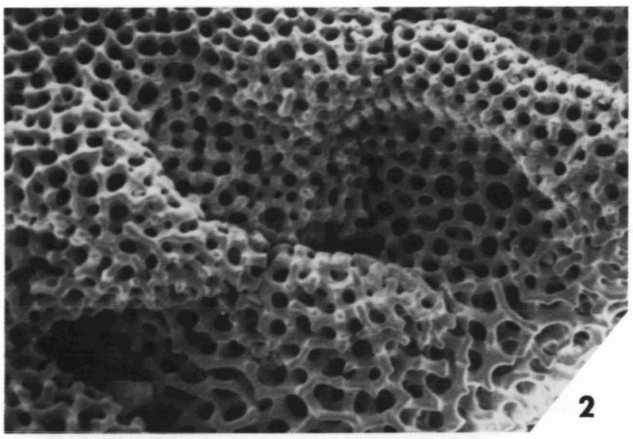
2

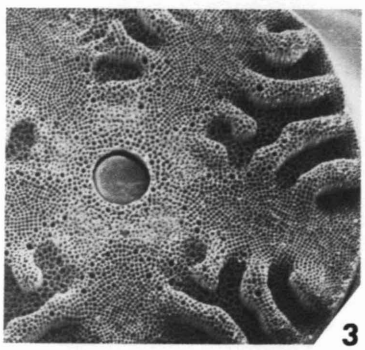
3

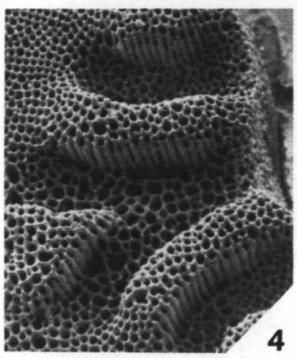
4


5

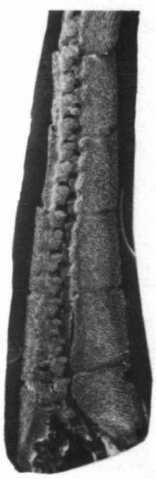
8


9

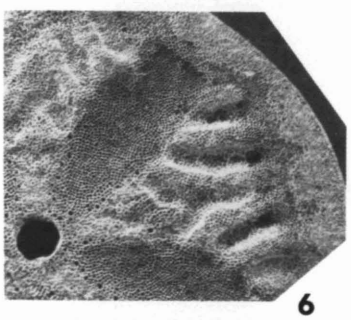
6

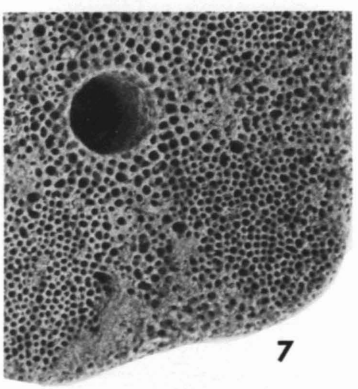
7

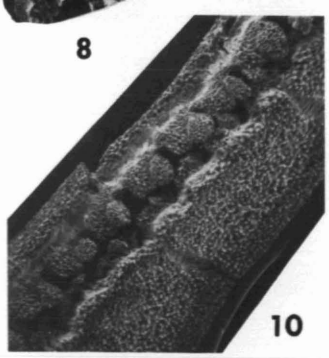
10

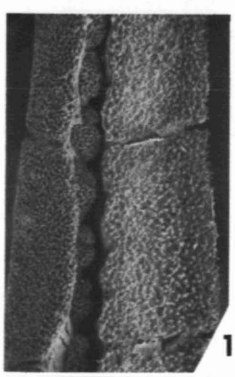
11

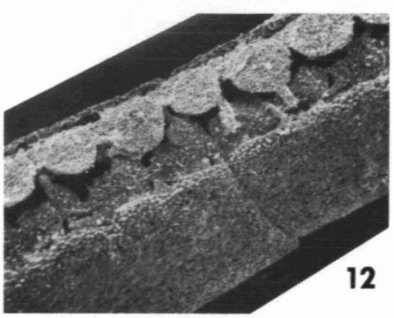
12